Max-Planck-Institut für Intelligente Systeme
(**ehemals Max-Planck-Institut für Metallforschung)**
Stuttgart

Simulation of the austenite-ferrite transformation; effect of applied stress

Mostafa Biglari

Dissertation
an der
Universität Stuttgart

Bericht Nr. 243
Januar 2013

Simulation of the austenite-ferrite transformation; effect of applied stress

Von der Fakultät Chemie der Universität Stuttgart zur Erlangung

der Würde eines Doktors der Naturwissenschaften (Dr. rer. nat.)

genehmigte Abhandlung

vorgelegt von

Mostafa Biglari

aus Teheran, Iran.

Hauptberichter:	Prof. Dr. Ir. E. J. Mittemeijer
Mitberichter:	Prof. Dr. S. Schmauder
Prüfungsvorsitzender:	Prof. Dr. Th. Schleid
Tag der Einreichung:	30. Oktober 2012
Tag der mündlichen Prüfung:	18. Januar 2013

MAX-PLANCK-INSTITUT FÜR INTELLIGENTE SYSTEME

(EHEMALS MAX-PLANCK-INSTITUT FÜR METALLFORSCHUNG)

INSTITUT FÜR MATERIALWISSENSCHAFT DER UNIVERSITÄT STUTTGART

Stuttgart 2012

Aan Elnaz

عقل گردی، عقل را دانی کمال عشق گردی، عشق را بینی جمال

When seeking wisdom, know fulfilment in wisdom.

When seeking love, see beauty in love.

Rumi

Contents

Chapter 1

Introduction

1.1 Solid state phase transformations

Many mechanical and engineering properties of a metal are determined by the microstructure of that metal. One way of changing or controlling the microstructure is a solid state phase transformation[1, 2]. In metal production many metals are subjected to heat treatments to induce desired phase transformations. To be able to engineer these heat treatments to produce the desired microstructure and the properties, fundamental understanding in solid state phase transformations is necessary. The driving force for a phase transformation can be understood by investigating thermodynamic differences between the parent phase to the product phase. The rate of transformation of a phase transformation is determined by the kinetics. Hence fundemental insights are gained by understanding the thermodynamics and kinetics of solid state phase transformation of interest.

1.2 Austenite-ferrite transformations

One of the most important solid-state transformations is the austenite (FCC, γ) $\rightarrow$ ferrite (BCC, α) transformation in iron-based alloys and steels. In pure iron this transformation can take place in two ways. If there is sufficient atomic mobility, the interatomic bonds in the austenite are broken and a *reconstruction* of atoms takes place to form ferrite*. In that case atomic jumps across the parent/product interface takes place in an uncorrelated fashion. If due to large undercooling the atomic mobility is reduced, the transformation takes place by *displacive* movement, where the atoms move in a correlated way, simultaneously to shear along certain directions and form martensite. Both these process are interface-controlled in the sense that process at the phase boundary control the transformation rate, albeit that somewhat confusingly the reconstruction type is sometimes called diffusional as short-range diffusion of the atoms through interphase boundary is necessary [8]. In the presence of substitutional alloying elements (e.g. Ni) or interstitial alloying elements (mostly important carbon),

*In scientific papers discussing the austenite-ferrite transformation in pure iron, some authors make a distinction between "equiaxial" ferrite and massive ferrite [3, 4], while others consider the two equivalent[3, 5–7]. "Equiaxial" ferrite as well as massive ferrite both grow through a reconstruction mechanism. It has to be noted that "equiaxial ferrite" is observed in experiments with higher amounts of impurities, while specimen with lower carbon contents in more recent studies show more columnar and coarse (i.e. massive) ferrite as consequence of a temperature gradient over the specimen [6, 7]. The difference between "equiaxial" ferrite and massive ferrite are explained by an increase in nucleation sites with increasing carbon contamination ($>$ 50 ppm). Thus the differences between equiaxial ferrite and massive ferrite in "pure" iron can be ascribed to a change in the nature of nucleation.

alloying elements can be more soluble in one phase than the other (i.e. a compositional difference between ferrite and austenite is energitically favourable), leading to phase transformation being controlled by long-range diffusion as the elements need to diffuse to or away from the advancing interphase bounary. These phenomena give rise to many possible mechanisms through which the austenite-ferrite transformation can take place. This wide range of mechanisms makes microstructural control possible. It is this microstructural control that enables for a large extent the versatile engineering of steels [8].

One type of mechanism for the austenite-ferrite transformation is the massive transformation. The massive transformation is characterized as an interface-controlled transformation, where the austenite ferrite hetero-interface moves through uncorrelated atoms jump across the phase boundary in the absence of long range diffusion (i.e. austenite and ferrite have the same composition) and no special Orientation Relationship (OR) between the austenite and ferrite phase [4, 9, 10]. The massive transformation occurs, when the chemical driving force for the transformation is high enough to allow nucleation and growth in a massive way, otherwise if the driving force is too low, the phase transformation will be controlled by long-range diffusion of elements to ensure the formed ferrite is energetically favourable. However, if undercooling is even higher even faster transformation such as the martensitic transformation can take place or the high-temperature phase is retained [11]. Due to only a short range reconstruction of the atomic bonds, these transformation are usually fast. As the interface mobility is governed by the diffusion of individual atoms through the interphase boundary, the austenite-ferrite interface is able to cross austenite grain

boundaries with no or little hindrance of the new OR between the parent and product phase.

The massive transformation is a nucleation and growth type of phase transformation, where first a nucleus is formed and subsequent growth takes place. There is an ongoing discussion, whether the massive nucleus is (partly) coherent with the parent phase. The first line of thought cites the observed lack of rational OR (i.e. along low index planes) between parent and product phase that no coherency exists between the nucleus and the matrix [4]. The other line of thought states that due to interface energy, for nucleation to take place at a significant rate, there has to be at least a partial coherency between nucleus and matrix. Subsequent growth of the nucleus can completely transform the original grain and the advancing interface can cross grain boundaries into grains with which there is no rational OR and hence rational OR cannot be observed at the final stage [9]. An often suggested growth mechanism for the massive transformation is the ledge mechanism, where atoms prefer to attach to steps thus grow the ledge, while ledges are formed slower [4, 9, 12].

As iron-based and steel workpieces often experience applied and internal stress the effects of loading on the transformation need to be understood. It was observed that even relatively small uniaxial loading (in the elastic range) have a significant effect on the massive austenite-ferrite transformations [13, 14]. In this project we are interested to gain more understanding on the interplay of stress and massive phase transformations, especially at the atomic length and time scales, in particulat recongnizing that in-situ experimental studies of the massive austenite-ferrite transformation are usually on a macroscopic level [6,

13–15] (experimental microscopic and atomistic data are commonly obtained *after* the transformation has been completed).

1.3 Atomistic simulations

Especially to obtain insight into the *atomic* mechanisms controlling the massive transformation computer simulations are necessary. Computer simulations have, over the last decades, become an essential tool to develop more knowledge about material science (e.g. see Ref. [16]).

The first step in creating a description at the atomic scale is the establishment of the energetic interactions atoms have with one another. This can be done *ab initio* by the Density Functional Theory (DFT) [17, 18], where the energy of the ground state can be calculated using the electron density. As the number of atoms which can be considered by its method is limited, other methods are necessary to give the energy involved for a larger ensemble of atoms. One important means to calculate the cohesive energy of such larger ensembles of atoms in metals is the Embedded Atom Method as developed by Daw and Baskes[19, 20]. Here the cohesive energy is calculated as the sum of the pair interaction between atoms and an additional embedding function, which accounts for the embedding of the individual atoms in the electron density at their position. The cohesive energy, E_{coh}, can then be described by

$$E_{\mathrm{coh}} = \sum_i [F_i(\sum_{i \neq j} f_j(r_{ij})) + \frac{1}{2} \sum_{i \neq j} \phi_{ij}(r_{ij})] \tag{1.1}$$

where the F_i is the embedding function for atom i, which is a function of the

local electron density, which is given by the sum of individual electron density contributions, f_j of atom j to the position of atom i, and ϕ_{ij} is the pair potential between atom i and j. The electron denstity contribution, f_j, and pair potential, $\phi_i j$, are both functions of the distance , r_{ij}, between atom i and atom j. The embedding functions, pair interaction and the electron density contribution can be optimised to a set of parameters obtained experimentally or from *ab-initio* calculations[21, 22]. The number of parameters taken into consideration and the cut-off distance for the interaction potential and electron density contribution are chosen such as to carefully balance computational costs against accuracy.

Most parameters used to optimise the EAM potential are usually correct for a specific temperature range. If such a potential is used to investigate phenomena at a different temperature, than for which these parameters are correct, it could very well be that the potential does not reflect the reality. For instance, most EAM potentials for iron are unidirectional, considering the austenite-ferrite transformation. This means that for MD simulations only one phase is energetically favourable over all temperatures (below the melting temperature), which is not the case in reality where in certain ranges bcc is more stable and in other temperature rangesr fcc is more stable[23].

1.3.1 Molecular Statics/Dynamics

Using an EAM potential the derivative of the energy as function of displacement of an atom in a configuration with other atoms (i.e. the force working on that atom) can be calculated. The calculated force can be used to find a local minimum for the energy as function of the configuration of atoms by using

e.g. Conjugate Gradient Method[24]. This method has been applied to find the interface structure between austenite-ferrite[22]. The drawback of minimizing the energy by this method is that the local minimum does not need to be the global minimum. It is readily conceived that a dislocation structure or interface reconstruction do not correspond to the local minimum of system formed by joining crystal blocks taken from infinite crystals.

If the forces working on an atom are known, they can also be used calculate the change in impulse and position for all atoms using Newtonian mechanics for a small time interval. By repeating this procedure the movement of atoms over time can be followed. The time scales accessible to MD simulations is in the order of only nanoseconds at moreover relatively high computational cost. Furthermore, considering the austenite-ferrite transformation, most MD simulations would, depending on the used interatomic potential and temperature, either exhibit a martensitic transformation or no transformation at all[23, 25–27]. Hence MD is generally not suited to investigate the effects of stress on the massive transformation, where large numbers of simulations are necessary.

1.3.2 Atomistic Monte Carlo

The Monte Carlo method has been developed by Ulam and Teller during the Manhattan project to describe stochastic phenomenona. The method took its name from the famous casino in Monaco, because the method makes use of random numbers/events. Nowadays the method is applied in numerous fields, because of low computational cost in comparison to deterministic simulations, and its ability to describe phenomena where the uncertainty about determining

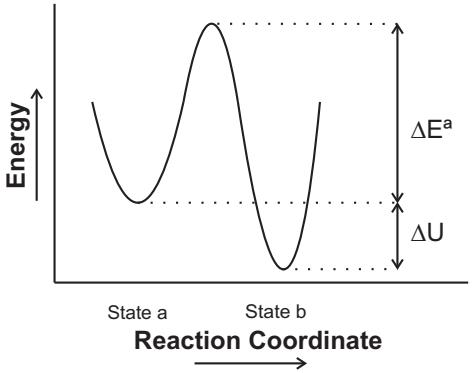

Figure 1.1: The energy of a transforming system as function of the reaction coordinate. The energy difference between state a and b is given by ΔU, while the activation energy for transforming from state a to state b is given by ΔE^a and the activation energy for the transformation back from state b to state a is given by $\Delta E^a + \Delta U$.

parameters is huge. The method involves the development of a catalogue of events, where each event has a certain likelihood of occurring. One event is picked randomly and the event executed. If necessary the catalogue of events is updated and again one event is picked, and so on. The process is repeated until a user-set threshold has been met. The degree of realism of Monte Carlo simulations depends heavily on how well the catalogue of events describes the events controlling the phenomena of interest. A good catalogue of events includes all cardinal events with an at least proportionally correct likelihood of happening.

For atomistic Monte Carlo the events are permutations between possible atomic configurations. These can be used to investigate the thermodynamics of interfaces by the Metropolis Monte Carlo method[28]. The method starts with an initial configuration of atoms s_i and permuting that configuration by

moving one or more atoms to create configuration $s_i + 1$. The new configuration $s_i + 1$ is accepted if it is energetically more favourable than s_i or if a random number is larger than the probability, $p = \exp(-\Delta U / k_B T)$, where ΔU is the energy difference between $s_i + 1$ and s_i, k_B is the Boltzmann constant and T is the simulation temperature (see Fig. 1.1). By repeating this procedure until convergence, a stable state for that simulation temperature can be found. Minor adjustments can be used to investigate other research topics, such as simulated annealing. In this method a global energetic minimum for a system (e.g. the austenite-ferrite interface) is sought for, by lowering the simulation temperature after each time convergence has been achieved (i.e. the proportion of atoms on unfavourable states has been lowered). This lowering is continued until T=0 and only energetically favourable jumps are allowed. This method has been used by Nagano and Enomoto[29] to find the interface structure and interface energy for the austenite-ferrite interface energy for flat austenite-ferrite interfaces.

With some adjustments this method can be changed to investigate the dynamic processes on the atomic scale by the so-called kinetic Monte Carlo (kMC). Instead of calculating one permutation of the initial state s_i, all possible permutations (i.e. states $s_i + 1a, s_i + 1b, ...$) are investigated at the same time. Then the jump rates to each of these states is calculated, which depend on the activation energy of each jump (cf. Fig. 1.1). One of the possible states is selected randomly with the likelihood of being chosen proportional to its individual jump rate. For investigating certain solid state phase transformations such as precipitation, it is possible to use rigid lattices, where a system is described by the crystal lattice sites of one phase and all the sites are occupied except for one.

The possible permutations are jumps of atom neighbouring the vacancy into the vacancy (cf. Fig. 1.2a).

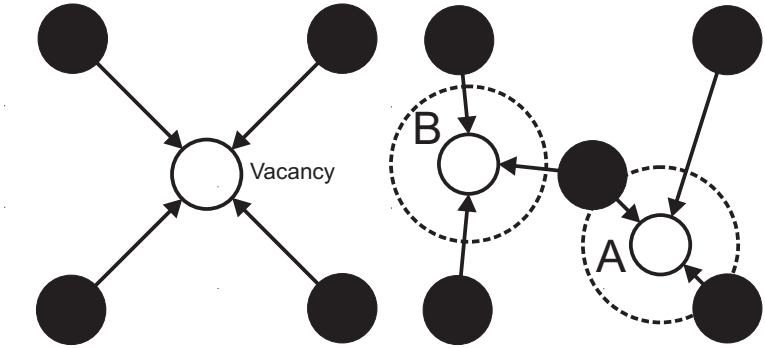

(a) Rigid lattice (b) Multi lattice

Figure 1.2: A schematic depiction of the Rigid lattice method (a) and the multi lattice method in two dimensions. The completely black circles represent occupied (crystal) sites, the arrows represents possible jumps and the unfilled circles represent empty sites. In the rigid lattice method all sites except for one site are occupied. Atoms neighbouring that vacancy can jump into that vacancy with a probability determined by the jump rate. In the multilattice method it is possible for atoms to jump to empty sites of another crystal lattice or random sites.

To investigate the kinetics of a solid state phase transformations of two crystalline phases by kMC, one crystal lattice providing the discrete sites is not enough, as the system should describe the lattice sites of the parent as well as the product phase. This is done by the multi-lattice kMC, where atoms can jump from occupied sites to empty sites (cf. Fig. 1.2b). These sites are given by the parent and the product phases and random sites. Random sites have been added to allow for irregular interface structures over the course of a simulation. This methods is very suited for the simulation of the massive austenite-ferrite trans-

formation, as coherent movement of atoms is not possible (i.e. no martenisitic transformations occur) and large number of simulations can be performed at relatively low computational cost[30, 31]. Hence the multi-lattice Monte Carlo method is used in this work.

1.4 Thesis Overview

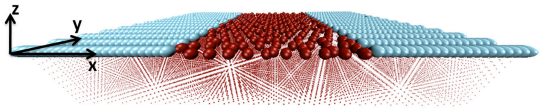

(a) Initial

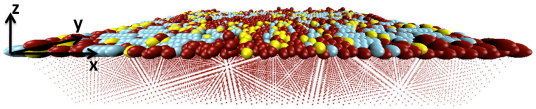

(b) Final

Figure 1.3: The $\gamma(11\bar{2})//\alpha(111)$ system before (a) and after (b) a multilattice kMC simulation with α atoms represented by maroon points and spheres, γ atoms by sky-blue spheres and atoms at random sites with gold spheres. The γ atoms above the interface layer are not shown to realize a clearer overview.

In this work the migration of the austenite-ferrite interface (austenite-ferrite transformation) under influence of loading is investigated. In chapter 2 the two-dimensional nucleation of ferrite at the ferrite-austenite interface under influence of uniaxial tension is investigated by Molecular Statics. The ledge mechanism has been suggested as a transformation mechanism for the massive transformation. Two-dimensional nucleation on top of an interface has been sug-

gested as mechanism for ledge generation [12]. The results are explained in terms of the volumetric misfit between austenite and ferrite, and compared with predictions by continuum methods.

Chapter 3 treats the growth of ferrite at the ferrite/austenite interface under influence of uniaxial loading by multi-lattice kMC (cf. Fig. 1.3). Two different interfaces OR are investigated. The changes in interface mobility were explained by the impact on local rearrangment for various amounts of loading, vacancy density and random sites density.

The results are explained by the amount of local rearrangement necessary for interface mobility in conjunction with amount applied uniaxial loading, the vacancy concentration and random site concentration.

In chapter 4, the massive austenite-ferrite phase transformation was simulated by means of multilattice kMC on an atomic scale for various states of loading: uniaxial, planar and hydrostatic. The effects of the different states of loading and of the vacancy concentration at the interface were discussed in terms of their impact on the necessary local rearrangement of austenite atoms to unblock unoccupied ferrite-lattice sites.

REFERENCES

[1] J. W. Christian. *The Theory of Transformations in Metals and Alloys*. Pergamon Press, Oxford, 2002.

[2] E. J. Mittemeijer. *Fundementals of Materials Science*. Springer-Verlag Berlin Heidelberg, 2010.

[3] M. Hillert, *Metall. Mater. Trans. A*, 15:411–419, 1984.

[4] T. Massalski, *Metall. Mater. Trans. A*, 33(8):2277–2283, 2002.

[5] T. Araki, M. Enomoto, and K. Shibata, *Mater. T. JIM*, 32:729–736, 1991.

[6] H. Kuroki and H. Y. Suzuki, *Mater. T. JIM*, 47:2449–2456, 2006.

[7] T. Ogawa, N. Harima, S. Takaki, and K. Abiko, *Mater. T. JIM*, 43:129–134, 2002.

[8] H. Bhadeshia, *Prog. Mater. Sc.*, 29(4):321 – 386, 1985.

[9] H. I. Aaronson, *Metall. Mater. Trans. A*, 33(8):2285–2297, 2002.

[10] H. I. Aaronson and V. Vasudevan, *Metall. Mater. Trans. A*, 33:2445–2470, 2002.

[11] T. Massalski. Massive transformations. In *Phase Transformations, ASM Seminar 1968,*, page 433, 1970.

[12] H. I. Aaronson, C. Laird, and K. R. Kinsman, *Scr. Metall.*, 2(5):259 – 264, 1968.

[13] Y. Liu, F. Sommer, and E. J. Mittemeijer, *Acta Mater.*, 57(9):2858 – 2868, 2009.

[14] G. Mohapatra, F. Sommer, and E. J. Mittemeijer, *Acta Mater.*, 55(13):4359 – 4368, 2007.

[15] Y. Liu, D. Wang, F. Sommer, and E. J. Mittemeijer, *Acta Mater.*, 56(15):3833 – 3842, 2008.

[16] D. Raabe. *Computational Materials Science*. Wiley-WCH Verlag Weinheim, 1998.

[17] P. Hohenberg and W. Kohn, *Phys. Rev.*, 136:B864–B871, 1964.

[18] W. Kohn and L. J. Sham, *Phys. Rev.*, 140:A1133–A1138, 1965.

[19] M. S. Daw and M. I. Baskes, *Phys. Rev. Lett.*, 50(17):1285–1288, 1983.

[20] M. S. Daw and M. I. Baskes, *Phys. Rev. B*, 29(12):6443–6453, 1984.

[21] R. A. Johnson and D. J. Oh, *J. Mater. Res.*, 4(5):1195–1201, 1989.

[22] Z. Yang and R. A. Johnson, *Model. Sim. Mater. Sc. Eng.*, 1(5):707, 1993.
[23] S. Tateyama, Y. Shibuta, T. Kumagai, and T. Suzuki, *ISIJ Int.*, 51(10):1710–1716, 2011.
[24] R. Fletcher and C. M. Reeves, *Comput. J.*, 7(2):149–154, 1964.
[25] C. Bos, J. Sietsma, and B. J. Thijsse, *Phys. Rev. B*, 73:104117–104124, 2006.
[26] K. Kadau, T. C. Germann, P. S. Lomdahl, and B. L. Holian, *Science*, 296(5573):1681–1684, 2002.
[27] S. Tateyama, Y. Shibuta, and T. Suzuki, *Scr. Mater.*, 59:971–974, 2008.
[28] N. Metropolis and S. Ulam, *J. Am. Stat. Assoc.*, 44(247):335–341, 1949.
[29] T. Nagano and M. Enomoto, *Metall. Mater. Trans. A*, 37:929–937, 2006.
[30] C. Bos, F. Sommer, and E. J. Mittemeijer, *Acta Mater.*, 53(20):5333 – 5341, 2005.
[31] C. Bos, F. Sommer, and E. J. Mittemeijer, *Acta Mater.*, 52(12):3545 – 3554, 2004.

Chapter 2

Energetics of nucleation at the austenite-ferrite interface; the effect of applied stress

M. Biglari Jr. and E.J. Mittemeijer

Abstract

The change of the cohesive energy upon formation of a two-dimensional ferrite particle at the flat interface of a ferrite(bcc)-austenite(fcc) bicrystal has been investigated by computer simulations for different amounts of uniaxial load applied normal to the interface (bcc(110)//fcc(111); bcc[001]//fcc[$11\bar{2}$] interface orientation). The atomic structure close to the interface was relaxed by the Conjugate Gradient method. The results have been discussed in terms of the effect of uniaxial loading on the parameters controlling the critical size of a particle, as, in particular, the interface energy and the misfit-strain energy. It is shown that an atomistic approach is crucial for understanding the energetics of nucleation at the ferrite/austenite interface.

2.1 Introduction

The austenite to ferrite phase transformation can control the microstructure and thus the properties of iron and steel workpieces. Therefore, knowledge about the behaviour and the structure of the austenite(fcc)/ferrite (bcc) interface is of cardinal importance. In many iron-based alloys the austenite-ferrite transformation can be of massive nature; i.e. a diffusion-less transformation controlled by uncorrelated jumps of atoms across the ferrite-austenite interface.

The ledge mechanism has been suggested as a transformation mechanism for massive transformations [1, 2]. Two-dimensional nucleation on top of an interface is a possible mechanism for ledge generation [3]. Thus a need exists to understand the effects of the parameters governing such nucleation phenomena.

During production and or usage, iron-based alloys can be subjected to applied stresses, which can influence the massive austenite to ferrite transformation [4, 5].

In the past computer simulations relaxing the austenite-ferrite system focused in particular on determination of the interface energy. These simulations concerned flat interfaces, the driving force for a γ-α transformation was set to zero and the role of applied stress was not considered[6, 7]. Nagano and Enomoto[7] used these simulation-obtained interface energies to determine the equilibrium shape of a nucleus. Chen et al.[8] also determined interface-energy values, but in the presence of a driving force favouring the ferrite phase. Hydrostatic stress was applied to force coherency in the interface plane between ferrite and austenite.

Bos et al.[2] used a bond counting model for describing the energetics of two-dimensional, ferrite nucleation, which allows neither relaxation of the interface nor the imposition of stress, as the interactions of the atoms in this model are only to a very limited extent distance dependent.

In this work the effects of uniaxial loading on two-dimensional nucleation of ferrite have been investigated on an atomic scale by Molecular Static simulations using an Embedded Atom Method (EAM). The effects of an applied load (uniaxial stress) were interpreted in terms of variation of the interface energy, the misfit-strain energy and the critical particle size.

2.2 Simulation Method

In the simulations performed during the course of this work the cohesive energy of a configuration of iron atoms was calculated adopting an EAM potential as proposed by Johnson and Oh[9]. This interatomic potential has been developed such that correct values for the elastic constants of the bcc phase are obtained and that the bcc phase is energetically favoured over the fcc phase.

The simulation starts by calculating the strains for each phase separately by applying a uniaxial load on an infinite crystal of each phase which is free to contract or expand normal to the direction of loading. A bicrystal is then created by joining a strained ferrite crystal block and a strained austenite crystal block such that a chosen crystallographic orientation relationship is satisfied. In the present work, the bicrystal had a bcc(110)//fcc(111); bcc[001]//fcc[$11\bar{2}$] interface orientation.

The distance between the crystal blocks is first set to equal to the inter-planar spacing for the ferrite phase in the direction normal to the interface. The direction normal to the interface is designated as the z-direction. The positive z direction is perpendicular to the interface in the direction of the austenite. As the periodicities of the two crystals generally do not match along the interface, the dimensions of the two crystal blocks in the x- and y-directions (of the order 15 nm) are chosen such that the lateral mismatch is small (less than 0.01 nm). Next, the bicrystal is relaxed iteratively by performing (i) minimization of the cohesive energy by means of the Conjugate Gradient (CG) method[10] implying adjustment of the individual atomic positions and (ii) subsequent minimization of the cohesive energy by moving the fcc crystal block along the z-axis; then step (i) is repeated, etc. This iterative procedure is continued until the difference in cohesive energy between the last two iterations is equal to or less than floating point precision.

The boundary condition for step (i) is that atoms beyond 40 Å from the circumference of the largest two-dimensional ferrite particle (see below) remain at their original positions. Periodic boundary conditions in the x- and y-directions were not imposed for step (i) because of the presence of a lateral mismatch (see above; also see Ref. [7]) and for step (ii) because the influence of the lateral edges of the bicrystal on the amount of movement in the z-direction is negligible.

Performing the above approach for relaxing a flat ferrite/austenite interface (no two-dimensional ferrite particle at the interface), the value for the cohesive energy thus obtained, is stored and is called $U_{\text{relaxed}}(0)$ (see what follows).

A ferrite particle with a radius r is inserted in the fcc layers at the centre of the interface of the unrelaxed bicrystal with a flat interface, by removing all fcc atoms in the transforming layers within radius r from the midpoint of the transforming fcc layers. Starting from the bcc sites closest to the midpoint, these removed fcc atoms are inserted at suitable bcc sites. An empty bcc site is suitable, if there is no other occupied fcc site within a distance d_{min}. If not all removed fcc atoms could be replaced at such bcc sites, these remaining removed fcc atoms will be inserted back at suitable fcc sites, until possibly all removed fcc atoms are replaced by bcc atoms or inserted back at fcc positions. If even then not all atoms removed have been replaced or inserted back, the distance d_{min} is made smaller and the search for suitable sites is restarted. Next the system thus created is relaxed by the procedure as described above and a value for the cohesive energy of the relaxed system with a two-dimensional ferrite particle at the interface is obtained, which is denoted by $U_{\text{relaxed}}(r)$.

For all simulations, uniaxial loading was applied in a direction normal to the interface. The bicrystal system was subjected to different stresses ranging from -1600 (MPa) to 1600 (MPa) in 400 (MPa) intervals. Simulations were performed with one, five and ten fcc layers transforming simultaneously by lateral growth parallel to the original bcc/fcc interface.

2.3 Results and Discussion

The interface structure of the flat austenite/ferrite interface after relaxation does not vary much under different amounts of applied stress. For the ferrite and

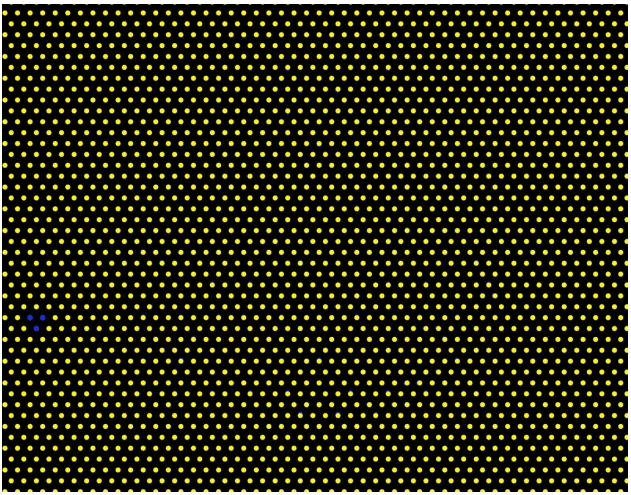

(a) γ layer

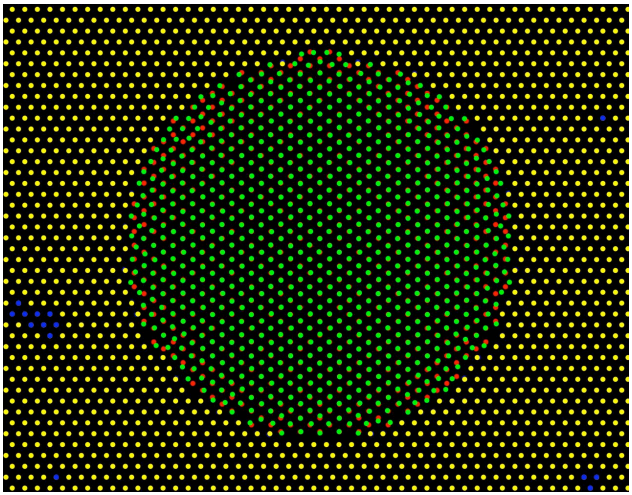

(b) Top nucleus layer

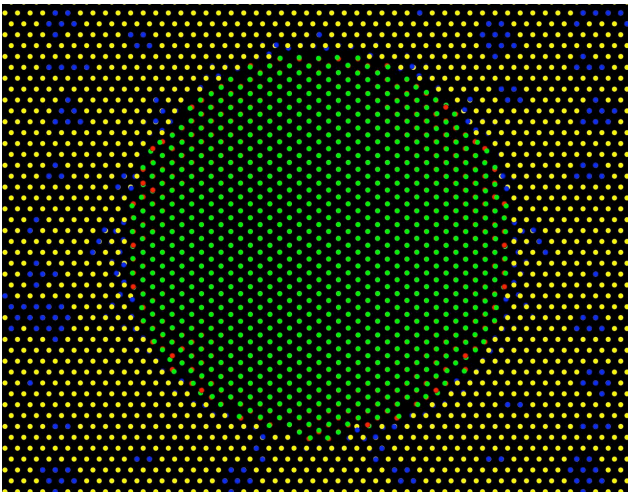

(c) Middle nucleus layer

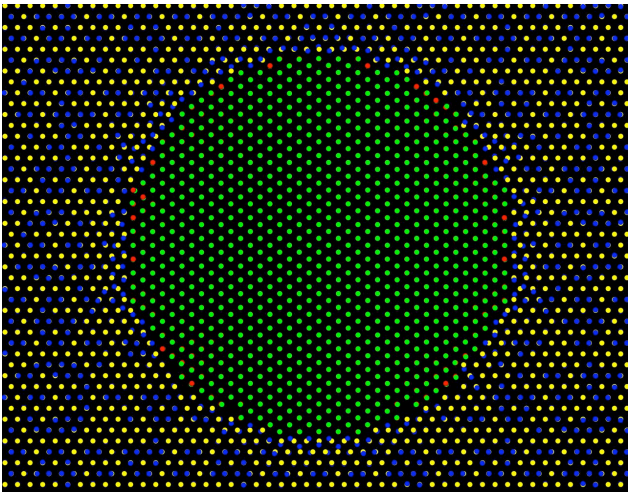

(d) Bottom nucleus layer

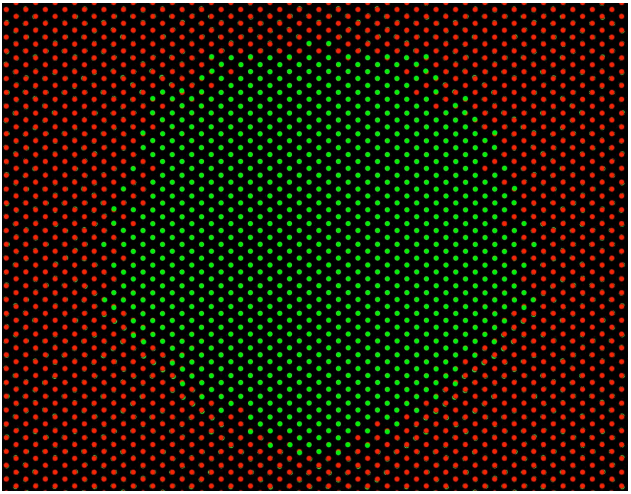

(e) α layer

Figure 2.1: Top view of individual atomic layers parallel to the original, flat austenite-ferrite interface: (a) the austenite layer immediately above the top of the ferrite particle; (b) the ferrite layer at the top of the particle and the laterally adjacent austenite layer; (c) the ferrite layer at the middle (i.e. half-height) of the particle and the laterally adjacent austenite layer; (d) the ferrite layer at the bottom of the particle and the laterally adjacent austenite layer, and (e) the ferrite layer immediately below the ferrite particle. The atom positions before and after relaxation have been visualised for the ferrite red (before) and green (after) and for austenite with yellow (before) and blue (after). If the positions of the atom before and after relaxation overlap such that they cannot be distinguished in the figure shown, only that position is shown (by colour) which has the higher value for the z-coordinate (also if the difference in z-coordinate value, before and after relaxation, is very small). The positive z direction is perpendicular to the interface in the direction of the austenite.

austenite atoms in the interface adjacent atomic layers, the movement is on average 5% of the ferrite nearest neighbour distance. The atomic structure at and around the ferrite particle before and after relaxation is visualised in Fig. 2.1. Upon relaxation the following observations can be made:

1. Atoms far from the ferrite particle have not moved significantly from the initial positions.

2. Almost all atoms in the ferrite particle have shifted upward in order to reduce the misfit at the top of the particle (Figs. 2.1b-d). In the ferrite layer below the particle atoms beneath the particle have moved upward as well, while ferrite atoms in the ferrite layer underneath the adjacent austenite have moved downward (Fig. 2.1e).

3. Ferrite and austenite atoms at and close to the circumference of the ferrite particle, as a consequence of the pronounced misfit along the circumference and as compared to the atoms at a flat interface, have moved more in order to relax the interface, leading to significant changes of their positions (as their lateral positions before and after relaxation are visible in Figs. 2.1b-d):

    - At the top of the ferrite particle the interface has relaxed primarily by movement of ferrite atoms at and close to the circumference of the particle (see Fig. 2.1b).
    - At the bottom of the ferrite particle the interface has relaxed primarily by movement of austenite atoms at and close to the circumference of the particle (see Fig. 2.1d).

Defining the energy difference of the relaxed bicrystal system with a ferrite particle/disc at the interface and the relaxed system with flat interface as $\Delta U_{\text{relaxed}}(r) \equiv U_{\text{relaxed}}(r) - U_{\text{relaxed}}(0)$ (cf. section 2.2), the results of the simulations for $\Delta U_{\text{relaxed}}(r)$ as function of r are shown in Fig. 2.2 for the case of five layers transforming at three different applied stress values: -1600, 0 and 1600 (MPa) (data points in Fig. 2.2).

The energy difference $\Delta U_{\text{relaxed}}(r)$, as function of r, comprises (at least) three different energy contributions[11, 12]. The inserted bcc particle will have a bulk cohesive energy different from the fcc phase volume it replaces. Interface energy is introduced proportional to the area of the circumference of the bcc particle/disc. Strain energy is inserted into the system, as a consequence of the different bulk densities of the fcc and bcc phases. The sum of these energy contributions can be given by

$$\Delta U_{\text{relaxed}}(r) = \rho_{\text{fcc}} \Delta U_{\text{fcc,bcc}} d_{\text{fcc}} \pi r^2 + 2\pi d_{\text{fcc}} \gamma r + C d_{\text{fcc}} \pi r^2 \qquad (2.1)$$

where $\Delta U_{\text{fcc,bcc}}$ is the difference in bulk cohesive energy per atom of the two phases, γ the interface energy of the circumference of the disc, d_{fcc} is the height of the disc, ρ_{fcc} is the density of the fcc phase and C is the misfit-strain energy per unit volume transformed fcc phase. The height of the disc, d_{fcc}, is given by the number of transforming layers multiplied with the distance between two fcc (γ) layers. The lines drawn through the simulated data points in Fig. 2.2 represent fits of Eq. (2.1) to the simulated data, with C and γ as fit parameters.

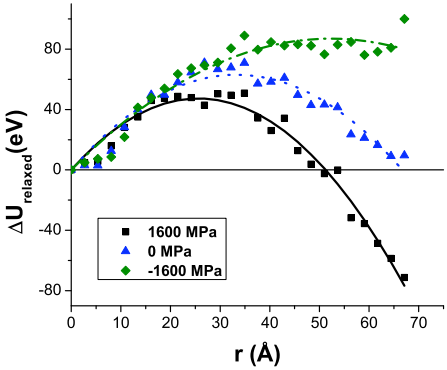

Figure 2.2: $\Delta U_{\text{relaxed}}$ as function of ferrite particle radius, r, for simulations with 5 transforming fcc layers at three different values of applied stress. The data points are results of the simulations; the lines drawn through the data are the results obtained by fitting Eq. (2.1) to the simulated data.

It follows from Fig. 2.2 that for all simulations Eq. (2.1) provides a good fit, except for the data pertaining to discs of (very) small radius. This can be understood as follows. For very small ferrite particles the positions of the atoms in the *relaxed* particle are quite similar to the positions of the fcc atoms removed upon insertion of the ferrite particle: the influence of the austenite surroundings is the larger the smaller the ferrite particle.

2.3.1 Interface energy and misfit-strain energy

The results obtained for the fit parameters misfit-strain energy C and interface energy γ are shown in Fig. 2.3 as function of the applied stress for various numbers of simultaneously transformed fcc layers (the distinction between in-

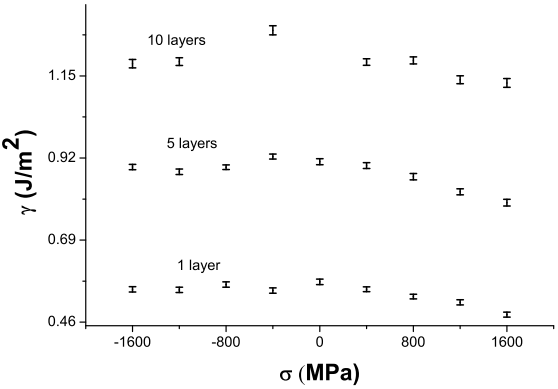

(a) γ

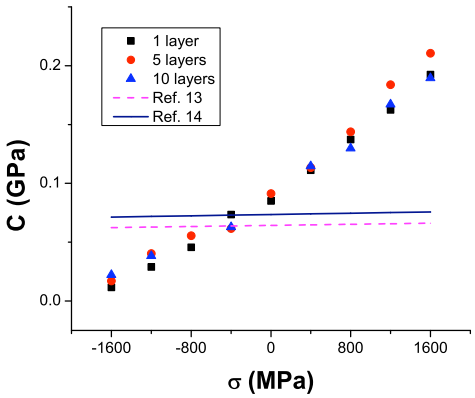

(b) C

Figure 2.3: The interface energy, γ (a), and the misfit-strain energy, C (b), as function of applied stress σ. Results obtained by fitting of Eq. (2.1) to the simulated data points (see Fig. 2.2). The error bars represent the standard error for the fit. The predicted values of C, also shown in (b) (note C in principle depends on σ), have been obtained according to the continuum physics approaches presented in Refs. [13] and [14].

terface energy and interface stress should be recognized*). The behaviour of γ as function of applied stress is the same for simulations with different numbers of transforming fcc layers, but the interface energy increases pronouncedly with an increase of the number of transformed layers. The interface energy of the system decreases with increasing applied tensile stress; in case of increasing applied compressive stress no distinct effect on the interface energy is observed. The strain energy per unit volume transformed, C, increases monotonously with increasing stress in both the compressive and the tensile stress regions. The effect of a variable number of transformed layers on C is relatively small. These results for γ and C can be discussed as follows.

The increase in interface energy with increase of the number of transforming layers is due to the corresponding decrease of the relative contribution of relaxation effects at and close to the circumference of the ferrite particle at the top and at the bottom of the ferrite particle (see under (iii) above). The saturation (maximum) value of the interface energy is approached relatively slowly because of

*Considering the following processes:

1. straining a relaxed bicrystal (of two joined, effectively infinite crystal blocks) leads to a change of energy ΔE_1;
2. straining, separately, of the two crystal blocks leads to a change of energy ΔE_2

The difference $\Delta E_1 - \Delta E_2$ is a measure for the difference of the interface stress and the interface energy. In the current calculations this difference is within the error range for the interface-energy values.

1. the favourable interaction of the ferrite atoms in the circumference in the bottom layer of the ferrite particle with the ferrite top layer at the original interface plus the relaxation effects (of austenite atoms) close to the circumference in the bottom layer of the ferrite particle (see Fig. 2.1d) and

2. the favourable interaction of the austenite atoms close to the circumference of the top layer of the ferrite particle with the austenite layer on top of the ferrite particle plus the relaxation effects (of ferrite atoms) close to the circumference in the top layer of the ferrite particle (see Fig. 2.1b).

As a result the interface energy increases relatively slowly with increasing the number of transforming layers. For example, considering 10 transforming layers, 2 layers at the top and two layers at the bottom of the nucleus are pronouncedly influenced by such interaction/relaxation effects.

A change in the numbers of transforming layers will not pronouncedly influence C as the misfit-strain energy per unit volume transformed will be practically constant upon increase (of the volume) of the ferrite particle, recognizing that C is mainly determined by the atoms in the bulk of the ferrite particle, as long as the number of bulk atoms in the ferrite particle is much larger than the number of atoms at the surface (circumference) of the ferrite particle; the atomic environment of the atoms in the bulk of the ferrite particle does not change significantly upon increasing the number of transforming layers.

The increase of C with increasing stress is a consequence of the associated rise of the absolute misfit strain, as follows. The volume misfit Δ can be given

as

$$\Delta = \frac{\Delta V}{V} = \frac{\rho_{\mathrm{fcc}}}{\rho_{\mathrm{bcc}}} - 1 \tag{2.2}$$

where ΔV is the difference of the volume of the unrelaxed ferrite particle and the volume, V, of the hole formed by removing the original austenite atoms. The effect of an uniaxial stress, σ, normal to the interface, on the number densities of atoms in the fcc and bcc crystal blocks, ρ_{fcc} and ρ_{bcc}, respectively, can be predicted using the lattice parameter a_i, the Young's modulus E_i and the Poisson ratio ν_i, of each phase i. Additionally assuming $1 \gg \sigma\frac{\nu_i}{E_i}$ and $1 \gg \sigma\frac{1}{E_i}$ for both phases, it is straightforwardly obtained

$$\Delta \approx \frac{2a_{bcc}^3}{a_{fcc}^3}\left(\frac{2\nu_{fcc}-1}{E_{fcc}} - \frac{2\nu_{bcc}-1}{E_{bcc}}\right)\sigma + \frac{2a_{bcc}^3}{a_{fcc}^3} - 1 \tag{2.3}$$

The slope of Δ as function of the stress σ depends on the difference of $\frac{2\nu_{fcc}-1}{E_{fcc}}$ and $\frac{2\nu_{bcc}-1}{E_{bcc}}$. The volume misfit Δ_0 for bicrystals under no stress follows from Eq. (2.3) with $\sigma = 0$. For the adopted interatomic potential, Δ_0 is negative. In the present case $\frac{2\nu_{fcc}-1}{E_{fcc}} > \frac{2\nu_{bcc}-1}{E_{bcc}}$. Then the absolute value of the volume misfit Δ increases with increasing tensile stress and decreases with increasing compressive stress (see Fig. 2.4).

Using these calculated values of Δ it may be asked if existing theoretical approaches might be applied to explain the results obtained in the simulations. The total elastic strain energy in a system composed of a homogeneous, incoherent, incompressible, ellipsoidal inclusion in a homogeneous isotropic matrix can be calculated according to Nabarro[13]. For the case of a homogeneous, incoherent, compressible, isotropic, ellipsoidal inclusion in a homogeneous, isotropic

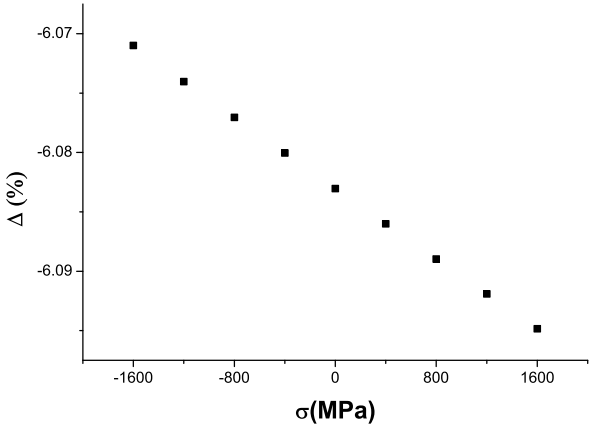

Figure 2.4: The volume misfit, Δ, as function of applied stress, σ.

matrix the total elastic strain energy can be calculated according to Kröner[14]. The results for C obtained for a disc shaped spheroid from both theoretical calculations have also been presented in Fig. 2.3b. Evidently, these theoretical approaches are incompatible with the results of the present simulations; the slope for C as function of applied stress given by the theoretical approaches is far less than the slope C compatible with the simulated data. Indeed, for the system studied, the ferrite particle is neither incompressible nor isotropic and the matrix is not a homogeneous, isotropic, single phase medium. It follows that existing, simple analytical treatments cannot be used to get even qualitative insight for the system studied in this paper. Moreover, considering Fig. 2.3b, as derived for the simulations, the misfit-strain energy becomes zero at a stress value where the misfit, as defined by Eq. (2.2) and as used in the (analytical) treatments discussed, does not equal nil. It can be suggested that in particular for small inclusions the necessity for excess, free volume at the phase bound-

ary, not taken into account in either of the mentioned theoretical approaches, but automatically accounted for in the present simulations, cannot be neglected for small inclusions in order to arrive at a realistic assessment of the misfit-strain energy.

To reveal the role of the transformation associated excess, free volume, additional simulations were performed, in the absence of varying applied stress, for the hypothetical case that both phases have the same density. Then the misfit as defined by Eq. (2.2) is zero. For this case, the values obtained in the simulations for $\Delta U_{\text{relaxed}}$ as function of r do not show a maximum for the range of r used in these simulations. Rather, $\Delta U_{\text{relaxed}}$ increases continuously for increasing r. Apparently the chemical driving force does not compensate the transformation suppressing interface energy and misfit-strain energy. Fitting of Eq. (2.1) to these data reveals that both γ and C are necessary as fit parameters to describe $\Delta U_{\text{relaxed}}(r)$. Thereby the occurrence of excess, free volume at the phase boundary of the ferrite particle is demonstrated, indicating the limited validity of Eq. (2.2) for expressing the volume misfit for small particles. It is noted here, as a side remark, that very recently it has been demonstrated experimentally that in nanocrystalline materials (i.e. materials with grain sizes of the order of the particles of (critical) size considered here) a relatively large amount of excess free volume occurs at the interfaces[15].

An increase of Δ, which is negative and thus becomes less negative, implies that the ferrite disc occupies more of the hole formed by the removed originally austenite atoms. At the interface of the ferrite particle and the austenite, the distance between bcc and fcc atoms will then be on average smaller and therefore

the atoms experience larger repulsive interactions. Hence the interface energy can increase upon decreasing the applied tensile stress (cf. Fig. 2.3a and Fig. 2.4). This process can proceed, until the bcc and fcc lattice sites at the circumference of the disc become too close (i.e. the bcc sites in the (circumferential) interface region have become unsuitable) and the algorithm then selects other sites to insert the atoms (see section 2.2). As a result the increase in the interface energy, γ, upon increasing Δ (i.e. Δ becomes less negative), attains a maximal value and stays more or less constant upon further increase of Δ (due to increase of compressive stress), as observed in Fig. 2.3a.

2.3.2 Critical size and shape

Traditionally, the critical size of the product ferrite particle, r_c, is defined as the size of a ferrite particle indicating that upon further growth a decrease in energy of the system occurs, which is the value of r where a maximum occurs in the curve of $\Delta U_{\text{relaxed}}(r)$ as function of r. The associated value of $\Delta U_{\text{relaxed}}(r_c)$ is called the energy of formation of a ferrite particle of critical size (= ferrite nucleus), ΔG^*. Such results for r_c and ΔG^*, as obtained from the simulations, are shown in Fig. 2.5. The critical size and the energy of nucleus formation increase for increasing the stress from compressive to tensile. Adopting the treatment leading to Eq. (2.1), the critical radius, r_c, is given by

$$r_c = \frac{-\gamma}{\rho_{\text{fcc}} \Delta U_{\text{fcc,bcc}} + C} \tag{2.4}$$

and the energy of nucleus formation is given by

$$\Delta G^* = \Delta U_{\text{relaxed}}(r_c) = \frac{-d_{\text{fcc}}\pi\gamma^2}{\rho_{\text{fcc}}\Delta U_{\text{fcc,bcc}} + C} \tag{2.5}$$

On the basis of the results obtained for γ and C and the interpretation provided in section 2.3.1, the dependencies of the critical nucleus size and the energy of nucleus formation on the applied stress can be understood as follows.

The value of the denominator in Eq. (2.4) and Eq. (2.5) is negative, because $\rho_{\text{fcc}}\Delta U_{\text{fcc,bcc}}$ is negative and, in absolute terms, larger than C, which is positive. As C increases for increasing stress (Fig. 2.3b), the absolute value of the denominator decreases, which results in an increase of both r_c and ΔG^* with increasing stress. The critical radius also increases with increasing the number of transformed layers, because the interface energy in the numerator of Eq. (2.4) increases (see Fig. 2.3a) while the other terms remain practically constant. The energy of nucleus formation increases even more pronouncedly with the number of transformed layers, because ΔG^* is proportional with the disc thickness, d_{fcc}, and the square of the interface energy while the other terms in Eq. (2.5) remain practically constant.

A shape factor for the particle of critical size can be defined as $f = r_c/d_{\text{fcc}}$. r_c is given by Eq. (2.4). As $\rho_{\text{fcc}}\Delta U_{\text{fcc,bcc}}$ and C (cf. Fig. 2.3b) are (practically) independent of d_{fcc}, it follows:

$$\frac{\partial f}{\partial d_{\text{fcc}}} = \frac{\gamma - d_{\text{fcc}}(\frac{\partial \gamma}{\partial d_{\text{fcc}}})}{d_{\text{fcc}}^2(\rho_{\text{fcc}}\Delta U_{\text{fcc,bcc}} + C)} \tag{2.6}$$

As, at constant applied stress, $(\gamma - d_{\text{fcc}}\frac{\partial \gamma}{\partial d_{\text{fcc}}}) > 0$ and $(\rho_{\text{fcc}}\Delta U_{\text{fcc,bcc}} + C) < 0$,

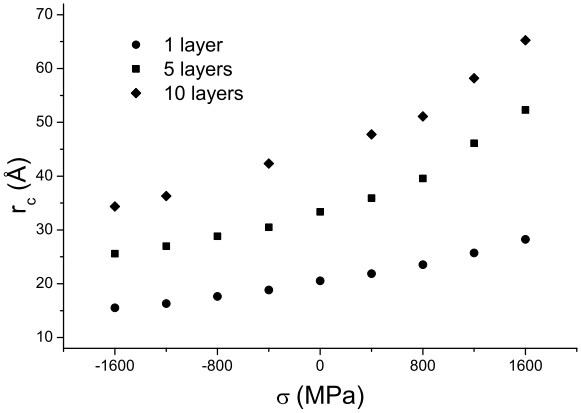

(a) Critical radius

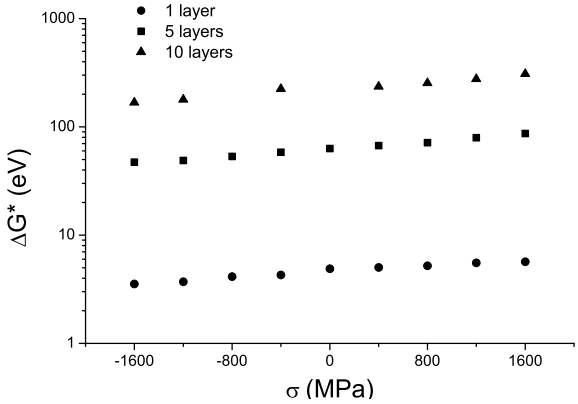

(b) Nucleus energy of formation

Figure 2.5: The critical radius, r_c (a), and the energy of nucleus formation, ΔG^* (b), as function of the applied stress, σ.

it is concluded $\frac{\partial f}{\partial d_{\text{fcc}}} < 0$: the shape of the particle of critical size changes from disc to needle upon increasing number of transforming layers.

2.4 Conclusions

- The dependence on applied stress of the change in energy of a ferrite (α) - austenite (γ) bicrystal, upon formation of a ferrite particle (disc) at the α/γ interface, could be expressed as the dependence of both the α/γ interface energy and the α/γ misfit-strain energy on applied stress.

- The continuum physics approach fails to describe the energy change as function of (ferrite) particle size for very small particles, because the influence of surrounding austenite matrix compels the α atoms, within the *relaxed* particle to take fcc-like lattice positions.

- The interface energy increases for decreasing applied tensile stress, because of the associated decrease of the distances between (neighbouring) bcc and fcc atoms at the interface, leading to increased repulsion at the interface. The interface energy is more or less constant for compressive applied stresses, because a minimal distance between the bcc and fcc atoms at the interface has to be complied with.

- The interface energy increases with increasing thickness of the ferrite disc, because the relative importance of the favourable interaction of the atoms at and close to the circumference of the top and bottom layer of the ferrite disc decreases with increasing thickness.

- The misfit-strain energy increases with increasing applied stress. This increase is very much more pronounced than as predicted by classical continuum physics treatments. In particular the misfit-strain energy becomes zero at an applied stress value where the classical misfit parameter (as defined by the bulk densities) does not equal nil. This is ascribed to the necessary presence of excess, free volume at the interface.

- Once the dependencies on applied stress of the interface energy and the misfit-strain energy have been determined by the atomistic computer simulation, a classical approach for the dependence of the critical particle size, r_c , and the associated energy of nucleus formation, ΔG^*, on interfacial energy and misfit-strain energy can be used to predict the dependencies of r_c and ΔG^* on applied stress.

Acknowledgements

One of us (M.B.) would like to thank the German Research Foundation (DFG) for financial support of the project within the Cluster of Excellence in Simulation Technology (EXC 310/1) at the University of Stuttgart.

REFERENCES

[1] H. I. Aaronson, *Metall. Mater. Trans. A*, 33(8):2285–2297, 2002.

[2] C. Bos, F. Sommer, and E. J. Mittemeijer, *Acta Mater.*, 52(12):3545 – 3554, 2004.

[3] H. I. Aaronson, C. Laird, and K. R. Kinsman, *Scr. Metall.*, 2(5):259 – 264, 1968.

[4] G. Mohapatra, F. Sommer, and E.J. Mittemeijer, *Acta Mater.*, 55(13):4359 – 4368, 2007.

[5] Y. Liu, F. Sommer, and E.J. Mittemeijer, *Acta Mater.*, 57(9):2858 – 2868, 2009.

[6] Z. Yang and R. A. Johnson, *Model. Sim. Mater. Sc. Eng.*, 1(5):707, 1993.

[7] T. Nagano and M. Enomoto, *Metall. Mater. Trans. A*, 37:929–937, 2006.

[8] J. Chen, D. Farkas, and W. Reynolds. Jr. In *Proceedings of International Conference on Solid-Solid Phase Transformations in Inorganic Materials '94*, Warendale, USA, 1994. TMS.

[9] R. A. Johnson and D. J. Oh, *J. Mater. Res.*, 4(5):1195–1201, 1989.

[10] R. Fletcher and C. M. Reeves, *Comput. J.*, 7(2):149–154, 1964.

[11] J. W. Christian. *The Theory of Transformations in Metals and Alloys*. Pergamon Press, Oxford, 2002.

[12] E. J. Mittemeijer. *Fundementals of Materials Science*. Springer-Verlag Berlin Heidelberg, 2010.

[13] F. R. N. Nabarro, *Proc. Phys. Soc.*, 52(1):90, 1940.

[14] E. Kröner, *Acta Metall.*, 2(2):302 – 309, 1954.

[15] Y. Kuru, M. Wohlschlogel, U. Welzel, and E. J. Mittemeijer, *Appl. Phys. Lett.*, 95(16):163112, 2009.

Chapter 3

Simulation of the massive austenite-ferrite transformation under uniaxial loading

M. Biglari Jr. and E.J. Mittemeijer

Abstract

The massive austenite-ferrite phase transformation has been simulated on an atomic scale by means of a multi-lattice kinetic Monte Carlo method. The simulated system involved a ferrite-austenite bicrystal under various uniaxial loads and for a variable number of vacancies at the interface. The results show that the massive transformation from austenite to ferrite is controlled by the local rearrangement of austenite atoms initially blocking unoccupied ferrite lattices sites. The growth mode is strongly dependent on the orientation of the interface. The effects of loading and vacancy concentration at the interface are discussed in terms of their impact on the necessary local rearrangement of austenite atoms. It is shown that local, relaxed clusters of atoms surrounding a vacancy play an important role for the kinetics of the transformation.

3.1 Introduction

The functional and structural engineering properties of a (metallic) workpiece are determined by its microstructure. A very important, much applied way of changing the microstructure of a solid material is to subject it to a solid state phase transformation [1, 2]. The massive austenite (γ) $\rightarrow$ ferrite (α) transformation is one such transformation for iron-based alloys. The massive transformation is characterized as an interface-controlled transformation, where the austenite-ferrite hetero-interface migrates through uncorrelated jumps of atoms across the phase boundary; i.e. in the absence of long range diffusion. No special Orientation Relationship (OR) between parent and product phase occurs[3–5].

In-situ experimental studies of the kinetics of the massive austenite-ferrite transformation are usually of macroscopic nature (i.e. length/volume or enthalpy changes are recorded)[6–11]; microscopic, atomistic data are commonly obtained only after the transformation has been completed, also because of the usually high transformation rates at the elevated temperatures; e.g. the austenite transformation is completed within a few seconds at temperatures in the range of 1090 - 1120 K[10]. The effect of uniaxial loading on the massive austenite-ferrite transformation has been investigated for FeNi alloys[9, 11]. It was shown that uniaxial compressive loading decreases the transformation induced deformation energy, so that the interface velocity increases with increasing compressive stress. For increasing uniaxial tensile loading it was shown that the transformation induced deformation energy increases, so that the interface

velocity decreases with increasing tensile stress. These effects were ascribed to anisotropy of the distribution of strain. As a uniaxial compressive load causes compression in the same direction as the load axis and expansion in the two normal directions, the transformation is facilitated in the directions normal to the load axis more than that the transformation is suppressed in the direction parallel to the load axis. For tensile loading the case is reversed: the transformation is suppressed in the two directions normal to load axis more than that transformation is facilitated parallel to the load axis[11].

The mechanisms controlling the massive transformation are inherently of atomistic nature. In view of the experimental difficulty to reveal the atomistic mechanisms in a direct way (see above) atomistic simulations can provide fundamental insight on the atomic time and length scales. Atomistic simulation of the austenite-ferrite phase transformation has been performed by either Molecular Dynamics (MD) methods [12–15] or kinetic Monte Carlo (kMC) methods [16–19]. Using a MD approach to investigate the massive transformation would need a driving force (which is given by / derived from the employed atomic interaction potential) for the transformation that low that the martensitic transformation does not occur[3], while the driving force should be high enough for the (desired) massive transformation to be completed in MD time scales[16]. These constraints can practically, for general interfaces, not be met. Therefore employing a kMC method, with an inherently non-coordinated movement of atoms and an accessibility to much longer time scales, appears to be very appropriate for simulation of the massive austenite-ferrite transformation.

KMC simulations by Bos et al.[16–19] show that the activation energy of

the interface mobility is governed by the amount of (excess) free volume and its distribution at the hetero-interface. The (excess) free volume is necessary to enable the movement of atoms away from austenite-lattice sites blocking ferrite-lattice sites. The free volume was varied in these studies by the insertion of vacancies at the interface region.

(Metallic) Workpieces /components in practice are subjected to applied or residual stresses, which can have great influence on (the kinetics of) phase transformations[10, 11]. The effects of stress on the massive austenite-ferrite transformation have not been investigated until now by atomistic simulations. The goal of this work is to investigate by kMC simulations the role of uniaxial tension and compression and excess free volume (by introducing vacancies) on the interface mobility of the austenite/ferrite interface.

3.2 Simulation of transformation kinetics

The (kinetic) Monte Carlo method involves the creation of a catalogue of possible events from which an event is chosen stochastically to happen and the consequences of the chosen event are evaluated. This approach has been adopted here to investigate the (interface) kinetics of the massive $\gamma \rightarrow \alpha$ phase transformation. The individual events considered in the simulation are the jumps of atoms from their initially position to an empty site in discretised space. In contrast with the common kMC simulations, where only one crystal lattice is used, a multilattice kMC method[16, 17] is used in this work: the possible positions of the atoms are provided by the sites of the crystal lattices of the parent phase and

the product phase plus a certain amount of so-called random sites that the atoms can take for an intermediate position between the crystal-lattice sites. Providing these intermediate positions is essential for a realistic description of the transformation interface. These random sites are distributed adopting a restrictedly random distribution method, by dividing the simulation volume in cubic cells with an approximate edge length of the second nearest neighbour distance in the γ phase and randomly distributing a fixed amount of random sites per cell.

The simulation loop starts with creating a list of all interface atoms. An atom is defined as an interface atom if it is adjacent to an atom of another type or if there is a vacancy on one of the neighbouring sites of its own type. For all these interface atoms all the possible jumps and corresponding jump rates are calculated. The jump rate k_i for jump i is calculated by

$$k_i = \nu_0 \exp[-\frac{E_i^a}{k_b T}] \tag{3.1}$$

where ν_0 is a frequency factor, E_i^a is the activation energy for jump i, k_b is the Boltzmann constant and T is the (absolute) temperature. The activation energy E_i^a is determined by $Q_i + \Delta U_i$, if the energy difference between the new configuration and the original configuration, ΔU_i, is positive, and by Q_i otherwise. Here Q_i represents the energy barrier for jump i, which is dependent on the local surroundings of the jumping atom.

The energy difference ΔU_i between two configurations is calculated via the Embedded Atom Method (EAM)[20, 21] using the Johnson-Oh potential[22].

The energy barrier Q_i is calculated with the Locally Activated Monte Carlo

(LAMC) method[23]. This is a procedure in which the jumping atom is moved in small steps along a straight line from its starting position to its destination. After each step, the jumping atom and the (here) fourteen closest atoms to the straight line between start and final position of the jumping atom are allowed to relax according to the conjugate gradient method[24]. During the relaxation the jumping atom is allowed to move only in the plane perpendicular to the straight line mentioned before. After the relaxation the cohesive energy of the system is stored. The difference of the cohesive energy associated with the state with the highest (= least negative) cohesive energy, along the path mentioned, and the cohesive energy associated with the start configuration is the activation energy E_i^a. If the cohesive energy difference ΔU_i is negative, the energy barrier Q_i is equal to activation energy, otherwise ΔU_i was subtracted from E_i^a to obtain Q_i. As determining values of Q_i during the Monte Carlo procedure would increase the simulation times dramatically, a neural network was trained to give a value for Q_i (output parameter) with a given set of input parameters. A suitable set of input parameters consists of the jump distance, the cohesive energies before and after the jump and the positions of the fourteen nearest neighbours.

A data set, containing the input parameters and the output parameter for 35000 jumps in the stress-free system, was used to train the neural network. Using a separate data set, containing the input parameters and the output parameter of another 5000 jumps in the stress-free system, to validate the trained neural network, yielded a normalized root mean square error for Q_i of less than two percent. For each of the states of stress applied in this work a data set, consisting of the input parameters and their corresponding output parameter as

calculated for a certain number of jumps by the LAMC method, was created. These data sets for strained bicrystals were used to validate the neural network, trained for the stress-free system, for application to strained bicrystals. It followed that the maximum normalized root mean square error in the value of Q_i is less than eight percent.

After the determination of the jump rates for all possible jumps for all interface atoms, these jump rates are summed up to a total jump rate K_{sum}

$$K_{sum} = \sum_{i}^{N} k_i \tag{3.2}$$

where N is the total number of jumps of all interface atoms. Next a random number R_1 between zero and K_{sum} is chosen. The jump selected to happen then is the first jump a for which the sum of its jump rate k_a and the jump rates for jumps with lower indices is equal to or larger than R_1:

$$\sum_{i}^{a} k_i \geq R_1 \tag{3.3}$$

The time Δt between two successive jumps can be calculated[25] using K_{sum} and a second random number R_2 between zero and one:

$$\Delta t = \frac{\ln(R_2)}{K_{sum}} \tag{3.4}$$

Here the basic simulation loop ends. The basic simulation loop is repeated until 50000 atomic jumps have been made. Next (i) unused random sites are redistributed, again according to the restrictedly random distribution described above and (ii) the γ crystal is moved to accommodate the volume misfit between

both phases. The misfit is accommodated by moving the γ lattice along the direction normal to the interface (the z-axis in Fig. 3.1), until the energy of the system is minimal. The simulation finishes if ten million atom jumps have been performed or the total number of atoms on α sites exceeds a certain number.

The growth rate (= number of net jumps towards α lattice sites divided by the corresponding time lapsed) was determined at moments that 400 atoms had transformed (i.e. had transferred from a γ lattice site to an α lattice site) by the total time lapsed for the transfer of those atoms. Each simulation was repeated a number of times under the same circumstances, with the differences being the seeds used for determining the random numbers R_1 and R_2 and the redistribution of the random sites. Results obtained from these similar simulations are presented as averaged outcomes. Thus the statistical significance of the results is improved. Simulations performed for different temperatures (cf. Eq. (3.1)) allow kinetic analysis by application of a weighted non-linear fit to the via simulation obtained transformation-rate data, according to[1]

$$r_{tf}(T) = \underbrace{M_0 \exp\frac{-\Delta G^a}{k_b T}}_{\text{M=interface mobility}} \; (1 - \exp(-\frac{|\Delta U_{\text{fcc,bcc}}|}{k_b T})), \tag{3.5}$$

where r_{tf} is the growth rate, T is the temperature, M_0 is a pre-exponential factor and ΔG^a represents the activation energy of the interface mobility. The fit parameters are M_0 and ΔG^a.

3.3 Simulation Settings

The lattice sites for the α phase and the γ phase were created by taking the unit cell for (strained) infinite single crystals, for two interface orientations: $\gamma(111)//\alpha(110);\gamma[11\text{-}2]//\alpha[001]$ and $\gamma(11\text{-}2)//\alpha(111);\gamma[110]//\alpha[11\text{-}2]$. Simulations were performed using 10, 5 or 2 random sites per cell (see begin of section 3.2). Vacancies were inserted by taking out γ atoms from the interface layer. Due to the different amounts of atoms in one layer for each of the ORs, the concentration of vacancies relative to the number of atoms in the transforming γ layer was almost the same if 5 vacancies were inserted for the $\gamma(11\text{-}2)//\alpha(111);\gamma[110]//\alpha[11\text{-}2]$ system with 980 γ atoms in one layer and 11 vacancies were inserted for the $\gamma(11\text{-}2)//\alpha(111);\gamma[110]//\alpha[11\text{-}2]$ system with 2240 γ atoms in one layer. The load was applied perpendicular to the interface and varied from -1600 (MPa) to 1600 (MPa) in steps of 400 MPa. A rectangular α nucleus was positioned at the middle of the x-axis in the γ interfacial plane (see Fig. 3.1a). The total number of occupied α sites necessary for finishing the simulation (see section 3.2) was taken equal to the number of α sites occupied initially plus the number of occupied ferrite sites resulting from the transfer of an amount of 80% of the atoms in the γ interface plane. If the simulations finished because of the total number of occupied α sites, rather then the total number of jumps (see section 3.2), the transformation was considered to be successful. The applied temperature ranged from 2028 K to 3042 K in steps of 253.5 K, with 48 repetitions at each temperature (see section 3.2). Statistical significance was shown not to be attained on the basis of only a few repetitions,

which implies a further advantage of kMC simulations over MD simulations, because of the great difference in computational cost.

3.4 Results and Discussion

3.4.1 General

All simulation runs resulted in a significant change of the distribution of the atoms over the available sites. Two types of end results were observed: (i) successful runs, exhibiting an increase in the number of occupied α sites and a decrease in the number of γ sites , in association with an increase in the number of occupied random sites (illustrated by Fig. 3.1b and Fig. 3.4a); (ii) unsuccessful runs, exhibiting an increase in the number of occupied random sites only, without distinct net transformation of γ to α (illustrated by Fig. 3.1c and Fig. 3.4b). The two different outcomes of the simulations are explained by the likelihood of a simulation leading to a specific configuration of occupied sites. In principle a simulation can lead to every configuration, except to configurations with a higher number of atoms on α sites than the total number of occupied α sites necessary for finishing the simulation (see section 3.3). The probability of a specific configuration as an end result of a simulation depends on the number of pathways leading to that configuration and the probability that such a pathway (i.e. the corresponding sequence of jumps) is followed. This leads to the following discussion.

During the course of a simulation atoms are jumping back and forth between all three kind of sites. The net change of the number of occupied sites of a

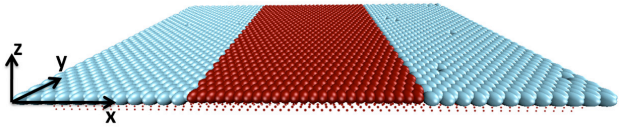

(a) Initial configuration

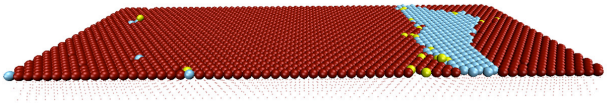

(b) Successful simulation

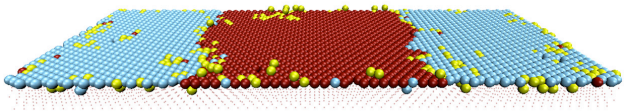

(c) Unsuccessful simulation

Figure 3.1: The $\gamma(111)//\alpha(110)$; $\gamma[11\bar{2}]//\alpha[001]$ system before (a) and after (b, c) simulation, with α atoms represented by maroon points and spheres, γ atoms by sky blue spheres and atoms at random sites with gold spheres. The γ atoms above the interface layer are not shown to realize a clearer overview. The final state of simulations was either a transformation of the layer (successful transformation) (b) or an interface where atoms mainly jumped to random sites (unsuccessful transformation) (c).

certain kind over a longer time scale depends on the difference of the total jump rate of jumps towards that kind of site and the total jump rate of jumps away from that kind of site over the same time scale. In the case of α sites the value of the driving force, as given by the EAM potential, implies that generally the rate of jumps towards α sites is higher than the rate of jumps away from α sites. In the case of random sites the initial absence of occupied random sites and the relatively high concentration of random sites lead to a net increase of occupied

random sites in all simulations: the occupation of random sites is generally not energetically preferred most, but, due to the sheer amount of possible jumps to these sites, the chance of a jump toward an empty random site becomes likely.

The reason, why simulations take a definite pathway, i.e. either a path leading to a net austenite-ferrite transformation or a path only leading to an increase of the number of occupied random sites, is due to a reinforcing effect experienced by the system once one of both types of pathways is chosen initially (by chance): the initial occupation of some empty α sites increases the likelihood that then more empty, neighbouring α sites will be occupied, which reinforcing effect stems from the change in ΔU_i: a jump of an atom on an austenite site or on a random site towards a neighbouring empty α site is more likely if the atom concerned is surrounded by an otherwise perfect α crystal lattice, because ΔU_i for such a jump is always negative. On the other hand, if, compared to the striven for occupation of α sites, more deviations occur (i.e. more neighbouring atoms are on random sites or γ sites instead of on α sites), then the likelihood of a jump towards an empty α site is relatively small, as it becomes more likely that the initial position of the atom concerned is relatively energetically favoured (i.e. the jumps towards an α site have a less negative (possibly even positive) ΔU_i). Therefore, by occupying empty α sites neighbouring empty α sites become more favourable, whereas the occupation of random sites, in particular by atoms stemming from α sites, will likely increase ΔU_i for jumps towards neighbouring empty α sites.

Varying the OR, the temperature, the load stress and/or the random site concentration can change the amount of successful simulation runs. This can be

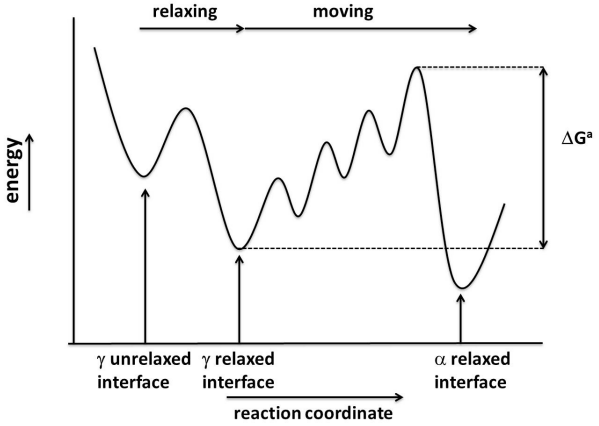

Figure 3.2: The activation energy of the interface mobility, ΔG^a, is given by the difference of the energy for the state with the least favourable configuration and the energy of the state with the relaxed γ/α interface (see text).

understood as follows. The transformation can be considered to occur in two steps: firstly, a relaxation of the γ/α interface occurs, and secondly, the relaxed α/γ interface moves in the direction of γ thereby establishing growth of α. As will be discussed in the sections below, in the initial stage, where only α and γ sites are occupied, some γ and/or α atoms in the interface region are on very unfavourable sites, in view of their local surroundings. Upon starting the simulation these α and γ atoms will then quickly move to a more favourable position, thereby (partly) relaxing the interface. Such a (partly) relaxed interface can be seen in Fig. 3.1b, where the occupied random sites are largely concentrated at the γ/α interface line in the transformation plane. This relaxed interface subsequently moves as there is a driving force for the transformation (cf. Fig. 3.2).

To be able to move the interface, a rearrangement of atoms on γ sites blocking an unoccupied α site is needed. Thus the interface moves by completing jump sequences, consisting of several unfavourable jumps to provide access to an unoccupied α site and thus make possible a final jump toward the unoccupied α site. The activation energy of the interface mobility, ΔG^a, is then given by the difference of the energy for the state with the least favourable configuration and the state with the relaxed interface (see Fig. 3.2).

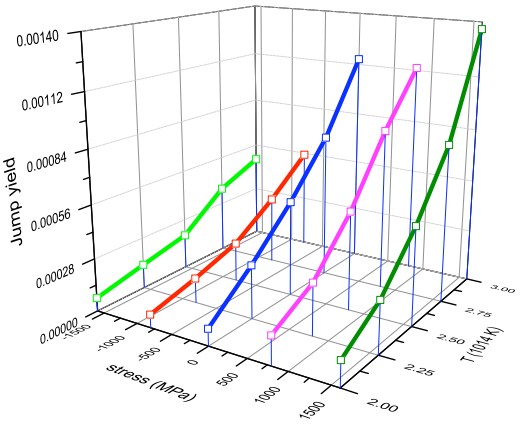

Figure 3.3: : The jump yield as function of applied stress and temperature for the $\gamma \rightarrow \alpha$ transformation at the $\gamma(111)//\alpha(110)$ interface with 11 vacancies inserted in the γ interface layer and five random sites per simulation cell. The data points represent the average jump yield of all successful simulation runs at the temperature and applied stress concerned.

Simulation runs are more likely successful if the necessary sequences to provide access to empty α sites become more likely, and vice versa. If there are at least two energetically unfavourable intermediate states involved in such se-

quences, an increase of the temperature leads to a higher chance of successfully crossing those energetically unfavourable intermediate states, yielding a higher jump rate (i.e. the net gain in occupied α sites divided by the total amount of jumps), increasing the chance of a successful simulation run (see Appendix B. in [17]).

An increase of the random site density leads to a smaller chance for a successful run as consequence of a higher chance for the jumping atom to occupy a random site. In such a case the transformation can even be stalled. The effects of loading and the different crystallographic ORs on the chance for a successful run will be discussed separately for each OR in sections 3.4.2 and 3.4.3.

In the following, the focus is on the effects of the applied load stress, in dependence on the crystallographic OR, on the transformation kinetics.

3.4.2 γ(111)//α(110) interface

Simulations with the $\gamma(111)//\alpha(110)$ interface yield two types of behaviour (cf. section 3.4.1) as illustrated in Figs. 3.1 and 3.4: (i) a transformation of γ to α ("successful completed run"; cf. Tables 3.1 and 3.2), showing an only slight increase of occupied random sites, with an almost exclusively lateral growth of the α phase in the plane of the nucleus (Figs 3.1b and 3.4b) and (ii) no net transformation of γ to α associated with an only slight increase in the number of occupied random sites (Figs. 3.1c and 3.4b).

The unsuccessful runs, i.e. no net γ to α transformation, happened more often for simulations (a) with 10 random sites per simulation cell, as compared to simulations with a lower concentration of random sites, (b) with applied com-

pressive stress and (c) at low temperatures (see Tables 3.1 and 3.2).

Table 3.1: The lowest temperatures, T, for which successful transformation was observed, and the total numbers of successful runs for various applied stresses. Results for each stress value as obtained for the $\gamma(111)//\alpha(110)$ interface from 240 simulations, with 48 simulations per each of five different temperatures, with *11 vacancies* inserted in the plane of the nucleus and with 10 random sites per simulation cell.

stress (MPa)	lowest T (x 1014 K)	successful runs of 240
1600	2	177
800	2	188
0	2	180
-800	2.5	65
-1600	2.5	22

Table 3.2: The lowest temperatures, T, for which successful transformation was observed, and the total numbers of successful runs for various applied stresses. Results for each stress value as obtained for the $\gamma(111)//\alpha(110)$ interface from 240 simulations, with 48 simulations per each of five different temperatures, with *no vacancies* inserted in the plane of the nucleus and with 10 random sites per simulation cell.

stress (MPa)	lowest T (x 1014 K)	successful runs of 240
1600	2	184
800	2	176
0	2	172
-800	2.25	30
-1600	2.25	17

The difference in the chance for successful transformation between cases of compressive loading and cases of tensile loading is due to the respective types of atomic rearrangement necessary to realize the transformation, as follows.

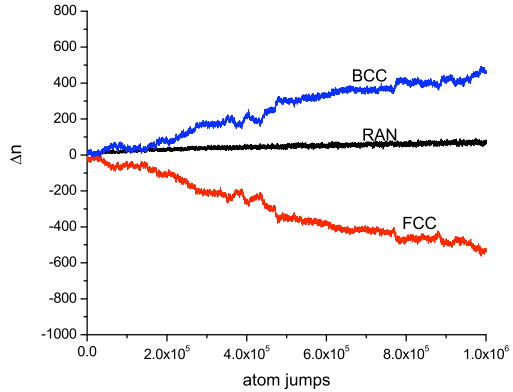

(a) Successful transformation

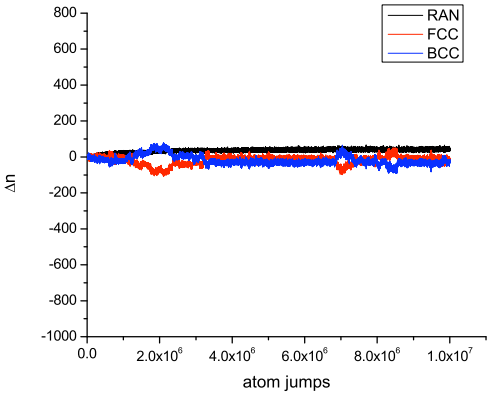

(b) Unsuccessful transformation

Figure 3.4: The difference in number of occupied sites, Δn, at specific time steps plotted for each type of site (BCC= α sites; FCC = γ sites; RAN = random sites) over the course of a simulation for (a) a typical successful transformation and (b) a typical unsuccessful transformation for the $\gamma(111)//\alpha(110)$ interface with no applied stress, with 11 vacancies inserted in the γ interface layer, and with five random sites per simulation cell at 2028 K.

Two types of atomic rearrangement at the γ/α interface can be distinguished: the relatively more common out-of-plane rearrangement and the less common in-plane rearrangement. The in-plane rearrangement is an atomic rearrangement where the γ atoms blocking unoccupied α sites jump to random sites *within* the transforming plane. This type of rearrangement is uncommon, because of the constraint placed on the necessary random sites to have almost the same height (same value for the z-coordinate; cf. Fig. 3.1) as the transforming plane. For the out-of-plane rearrangement the blocking γ atoms not only jump in the x- and/or y-directions, but also in the z-direction to achieve access to initially blocked α sites. This type of rearrangement is thus more common than the in-plane rearrangement as the requirement for the first type of rearrangement for random sites to lie within the transformation plane is relaxed.

Under applied tensile stress, perpendicular to the original α/γ interface, jumps parallel to the direction of loading are relatively more favourable than jumps normal to the direction of loading, whereas jumps normal to the direction of loading are suppressed. Hence the more common out-of-plane rearrangement (see above) becomes relatively more likely and can overcompensate the suppression of the in-plane rearrangement. Under applied compressive stress, perpendicular to the original α/γ interface, jumps normal to the direction of loading are relatively more favoured, which favours the less common in-plane rearrangement pathways (see above). Hence the transformation has to be realized via less likely transformations paths in the case of compressive loading as compared to the case of tensile loading and therefore the number of successful runs is higher under tensile loading than under compressive loading (cf. Tables 3.1

and 3.2). This conclusion is compatible with the observation that the jump yield (i.e. the ratio of the number of jumps to ferrite sites and the total number of jumps) is higher for tensile loading than for compressive loading (cf. Fig. 3.3).

3.4.2.1 The Activation Energy, ΔG^a

For this interface orientation simulations with ten random sites per simulation cell did not yield enough successful runs to allow a meaningful fit of Eq. (3.5) (see above). Sufficient numbers of successful transformation occurred for simulations with two and five random sites per simulation cell. The results obtained for ΔG^a by fits of Eq. (3.5) to these data have been presented as function of applied stress in Fig. 3.5. As compared to the results in Ref. [19], where no applied stress was considered and where the crystal-lattice parameters were chosen such that there was an equal planar density for α and γ sites at the interface plane, the absolute value of the activation energy in the present work obtained in absence of applied stress is higher, which can be understood as a consequence of the higher planar and bulk densities of α and γ sites, involving a lower value of free volume per atom for the simulations in the present work.

The values determined for the activation energy as obtained from simulations with two random sites per simulation cell are somewhat larger than those obtained from simulations with five random sites per simulation cell. This is consistent with results obtained in Ref.[19] where applied stress was not considered.

Generally, the influence of an increase of the concentration of random sites

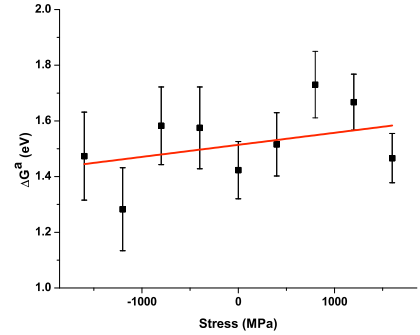

(a) No vacancies

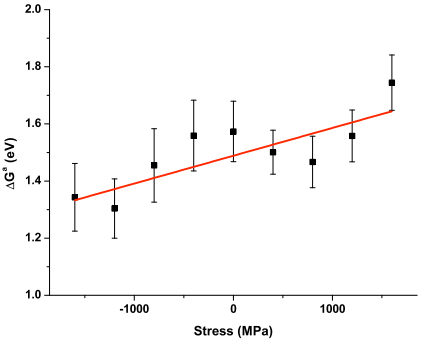

(b) 11 vacancies

Figure 3.5: The activation energy of the interface mobility, ΔG^a, as function of applied stress. The results in (a) are based on simulations for the $\gamma(111)//\alpha(110)$ system with five random sites per simulation cell and with no vacancies inserted in the transformation layer. The results in (b) are based on simulations for the $\gamma(111)//\alpha(110)$ system with five random sites per simulation cell and with 11 vacancies inserted in the transformation layer. The data points have been obtained by non-linear least-squares fitting of Eq. (3.5) to the transformation rates obtained from simulations as function of temperature. The error bars assigned to the data points indicate the standard error for the non-linear fit of Eq. (3.5). The straight lines drawn represent linear fits to the data points in the figure

Table 3.3: Results obtained for the straight line fitted to the data points obtained for the activation energy of the interface mobility, ΔG^a, as function of applied stress for the $\gamma(111)//\alpha(110)$ system. Ran and Vac designate the number of random sites per simulation cell and the amount of vacancies inserted in the transformation layer, respectively; Slope and SE slope correspond with the slope of the fitted straight line and its standard error; Intercept and SE intercept correspond with the intercept of the fitted straight line with the ordinate at zero stress and its standard error. A "yes" in the column "Check" means that the slope and the intercept of the fitted straight line were equal, within the standard error range, to the results of the fit performed after leaving out the data point with the largest residual.

Ran	Vac	Slope (eV/MPa)	SE Slope (eV/MPa)	Intercept ($\sigma = 0$) (eV)	SE Intercept (eV)	Check
2	0	-1.9e-5	4.1e-5	1.673	0.042	Yes
2	11	3.0e-5	3.2e-5	1.621	0.033	Yes
5	0	4.3e-5	3.9e-5	1.514	0.042	Yes
5	11	9.7e-5	3.4e-5	1.489	0.034	Yes

on the activation energy of the interface mobility is associated with the two following antagonistic effects:

(i) An increase in random site density leads to more freedom for the atoms to rearrange and thus more easy paths for the transformation from γ to α become available. Increasing the random site concentration leads to intermediate states that are relatively more favourable energetically, which leads to a lower effective activation energy of the interface mobility.

(ii) An increase in random site density leads to a more extended relaxation of the α/γ interface (cf. section 3.4.1). Moving such a relaxed α/γ interface requires relatively more rearrangement in the the γ phase right in front of the α/γ interface. This extra rearrangement involves a higher activation energy of the interface mobility (cf. Fig. 3.2).

The net result of the two effects depends on the interface orientation. For the present interface an increase in the random site density corresponds with a decrease in the activation energy of the interface mobility (Table 3.3). For the other interface (cf. section 3.4.3) an increase in the random site density corresponds with an increase in the activation energy of the interface mobility (Table 3.4).

To investigate the trend of ΔG^a as function of stress linear fits to the data in Fig. 3.5 were made. As linear fits are sensitive to outliers and the number of data points is low, every fit was checked for consistency by repeating the linear fit after leaving out the data point with the largest residual. If the slopes and parts cut from the ordinates (at zero stress) for both fits are equal within the standard error ranges, the results of the fits were accepted. The results of these fits have been gathered in Table 3.3.

Simulations executed with larger random site densities yield results which show a distinct change in the activation energy as function of the applied stress, while simulations with smaller random site densities yield results showing no significant dependence of the activation energy on applied stress (Table 3.3). A higher random site density provides more possible transformation pathways, and thus more opportunities to express, by changes in the local surroundings of the jumping atoms, a response to the applied stress.

For the case of five random sites per simulation cell, with and without vacancies, the activation energy of the interface mobility is raised upon increasing the load stress (compressive to tensile; see Fig. 3.5). This effect can be discussed as follows. Compressive loading in the direction perpendicular to the interface

has two antagonistic effects: (i) a decrease in the free volume and (ii) a decrease in the planar atomic number density in the plane of growth (i.e. parallel to the interface). The former effect increases the activation energy of the interface mobility, whereas the latter effect decreases it. For tensile loading the effects are reversed. Therefore it can be concluded that, for the interface orientation considered with its planar growth mode, it is the decrease of the planar atomic number density upon increasing load stress (compressive $\rightarrow$ tensile), which predominates the change of the activation energy of the interface mobility with the change of stress.

The vacancy density has a profound influence on the transformation. A higher vacancy concentration leads to a more “regular” behaviour of the activation energy as function of applied stress. More "regular" behaviour means smaller differences in the results obtained from a series of simulations carried out for the same applied stress (see standard error values given in Table 3.3), implying that the rate determining pathways (series of atomic jumps) become more equal.

Simulations, performed with 5 random sites per simulation cell and 11 vacancies inserted in the transformation layer, yielded a (linear) dependence of the activation energy of the interface mobility as function applied stress, of higher slope, but of equal intercept (at zero stress), as compared to such behaviour determined from comparable simulations with no vacancies (cf. Table 3.3). Hence, in case of a compressive load, vacancies lower the activation energy of the interface mobility, whereas in case of a tensile load, vacancies increase the activation energy. This role of vacancies can be explained as the net outcome of

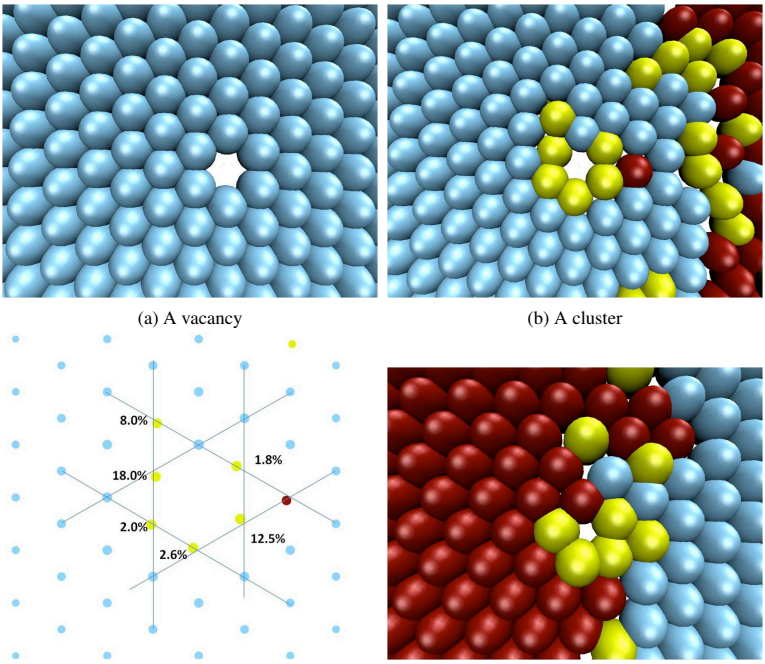

(a) A vacancy (b) A cluster

(c) A cluster (d) Cluster at interface line

Figure 3.6: Atomic arrangement around a vacancy at the $\gamma(111)//\alpha(110)$ interface. Sky blue, maroon and gold atoms are at γ, α and random sites respectively. Atoms surrounding an unrelaxed vacancy (a) can jump to random sites surrounding the vacancy and form a cluster of occupied random sites (b). The relaxed nature of the atomic arrangement around the vacancy is illuminated by (c) where the lines drawn connect γ lattice sites, and the numbers given indicate the deviation in z-direction (relative (in %) to the (111) lattice-plane spacing in γ) from an ideal γ lattice site for the 248 atoms concerned. Such clusters at the γ/α interface line (d) hinder the γ/α interface migration by exerting a pinning/drag force (see text).

two opposite effects: An increase of vacancy concentration is associated with (i) a decrease in the atomic number planar density in the plane of growth, which facilitates the transformation, and (ii) an increase of the number of stable clusters of occupied random sites surrounding a vacancy in the plane of growth, which suppresses the transformation. These clusters of occupied random sites are formed by atoms moving into random sites around a vacancy, thereby partly relaxing the stress field around a vacancy. In the bulk of a crystal every crystal-lattice site is equivalent for a vacancy, i.e. ΔU_i is zero for a vacancy jump in the bulk. This is not the case at the interface, where some lattice sites are more favourable for vacancies than others due to the irregular (atomic) structure of the interface. Hence, the vacancies prefer to be (to stay) at specific places at the interface and thus these clusters of occupied random sites surrounding a vacancy are formed (see Fig. 3.6). Such clusters at the interface can exert a pinning/drag force on the (moving) interface. Thus the moving interface either has to "push" the vacancy away into a less favourable site or bow around it. The transformation enhancing effect by increasing vacancy concentration is thereby opposed by the formation of interface-pinning clusters.

As vacancies are strongly bound to the interface (see above), atomic rearrangement of a cluster, leading to the movement of a such a cluster (i.e. movement of the vacancy) is primarily realized by *in-plane* rearrangements. As discussed in the begin of section 3.4.2, in-plane rearrangement becomes more likely under compressive loading and less likely under tensile loading. Hence, under compressive loading the (lateral) movement of such a cluster (i.e. movement of the vacancy) becomes more likely, so that it is able to facilitate

the transformation with the vacancy-associated free volume. Reversely, under tensile loading the mobility of the vacancy within the plane of transformation decreases, thereby suppressing the transformation. Hence it can be concluded that effect (ii) predominates the change of activation energy of transformation in case of increasing tensile loading, whereas effect (i) predominates that change in case of increasing compressive loading. The stress at which these effects ((i) and (ii)) cancel each other out is close at zero stress (cf. Table 3.3).

3.4.3 γ(11-2)//α(111) interface

For this interface orientation, the α (bcc) nucleus did not only grow laterally: a rough interface with γ was formed (i.e. a more isotropic growth of α occurred; see Fig. 3.7). In this case all simulation runs were successful, i.e. led to $\gamma \rightarrow \alpha$ transformation of an amount of atoms equivalent to 80% of the remaining γ atoms in the plane of nucleation. The results for ΔG^a, as determined by fitting Eq. (3.5) to the transformation rate data, are shown in Fig. 3.8. The slopes and the intercepts of the ordinates at zero stress of the straight line fitted to the data points in Fig. 3.8 have been gathered in Table 3.4.

The (much) higher chance for a successful simulation for the γ(11-2)//α(111) interface, as compared to the γ(111)//α(110) interface, is ascribed to the more "open" structure of the γ(11-2)//α(111) interface as compared to the γ(111)//α(110) interface. The empty α sites at the γ(11-2)//α(111) interface are less blocked and therefore the $\gamma \rightarrow \alpha$ jump yield (cf. section 3.4.2) is increased and the activation energy of the interface mobility is decreased significantly (cf. the ΔG^a data presented in Figs. 3.5 and 3.8).

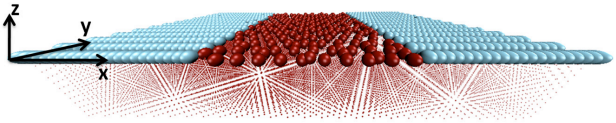

(a) Initial

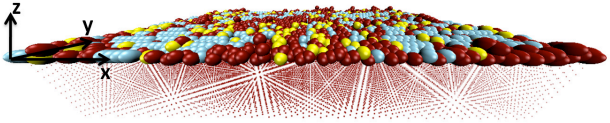

(b) Final

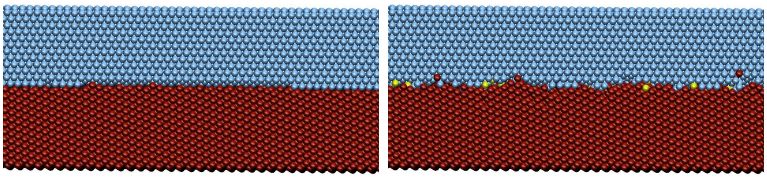

(c) Initial (d) Final

Figure 3.7: The $\gamma(11\bar{2})//\alpha(111)$ system before (a) and after (b) successful (see text) simulation with α atoms represented by maroon points and spheres, γ atoms by sky-blue spheres and atoms at random sites with gold spheres. The γ atoms above the interface layer are not shown to realize a clearer overview. The cross sections (c) and (d) illustrate the roughness of the interface that has developed in the final state (d) as compared to the initial state (c).

3.4.3.1 The Activation Energy, ΔG^a

The activation energy of the interface mobility increases with increasing concentration of random sites (cf. data for the "intercept" in Table 3.4), in contrast with what is observed for the more dense $\gamma(111)//\alpha(110)$ interface, as a consequence of a corresponding increased relaxation of the relatively "open" $\gamma(11\text{-}2)//\alpha(111)$ interface. As discussed in section 3.4.2.1, increasing the number of random sites is associated with two for ΔG^a antagonistic effects: increase of the number of favourable transformation pathways and an increased relaxation of the interface. In the case of the $\gamma(111)//\alpha(110)$ interface with a limited amount of relaxation of the interface preceding interface movement (growth of α), the first effect prevails, whereas the second effect is dominant for the $\gamma(11\text{-}2)//\alpha(111)$ interface. The relatively pronounced relaxation of the $\gamma(11\text{-}2)//\alpha(111)$ interface is also illustrated by the observation that, at the start of the transformation, initially the number of occupied α sites drops and the number of occupied random sites increases sharply, followed, of course, by an increase of the number of occupied α sites (cf. Fig. 3.9).

Loading has only a distinct influence on the activation energy if vacancies are present at the interface and an appreciable density of random sites occurs (see results for ten random sites per simulation cell in Table 3.4). When no vacancies are present at the interface the transformation is controlled by the (interface intrinsic) amount of free volume. Although the amount of free volume changes upon loading, due the "open" nature of this interface orientation, the effects on the activation energy, caused by the stress-induced change in the amount of free

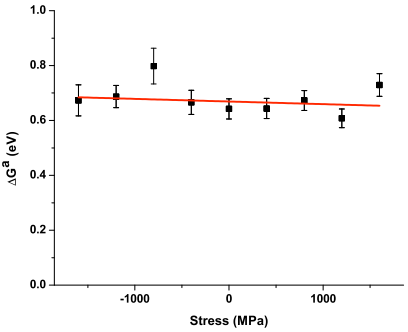

(a) 5 Random Sites

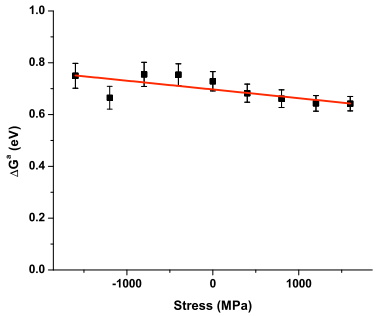

(b) 10 Random Sites

Figure 3.8: The activation energy of the interface mobility, ΔG^a, as function of applied stress. The results in (a) are based on simulations for the $\gamma(11\bar{2})//\alpha(111)$ system with five random sites per simulation cell and with five vacancies inserted in the transformation layer. The results in (b) are based on simulations for the $\gamma(11\bar{2})//\alpha(111)$ system with ten random sites per simulation cell and with five vacancies inserted in the transformation layer. The data points have been obtained by non-linear least-squares fitting of Eq. (3.5) to the transformation rates obtained from simulations as function of temperature. The error bars assigned to the data points indicate the standard error for the non-linear fit of Eq. (3.5). The straight lines drawn represent linear fits to the data points in the figure.

Table 3.4: Results obtained for the straight line fitted to the data points obtained for the activation energy of the interface mobility, ΔG^a, as function of applied stress for the γ(11-2)//α(111) system. Ran and Vac designate the number of random sites per simulation cell and the amount of vacancies inserted in the transformation layer, respectively; Slope and SE slope correspond with the slope of the fitted straight line and its standard error; Intercept and SE intercept correspond with the intercept of the fitted straight line with the ordinate at zero stress and its standard error. A "yes" in the column "Check" means that the slope and the intercept of the fitted straight line were equal, within the standard error range, to the results of the fit performed after leaving out the data point with the largest residual.

Ran	Vac	Slope (eV/MPa)	SE Slope (eV/MPa)	Intercept ($\sigma = 0$) (eV)	SE Intercept (eV)	Check
5	0	-2.9e-5	1.3e-5	0.63	0.014	No*
5	5	-1.0e-5	1.4e-5	0.66	0.014	Yes
5	10	0.7e-5	1.4e-5	0.68	0.015	Yes
10	0	-0.8e-5	1.2e-5	0.69	0.012	Yes
10	5	-3.4e-5	1.2e-5	0.70	0.013	Yes
10	10	-2.8e-5	1.3e-5	0.72	0.013	Yes

* Test result: Slope 0.1e-5; SE Slope 1.7e-5

volume, are negligible (cf. result for ten random sites per simulation cell and no vacancies for the γ(11-2)//α(111) interface in Table 3.4); this is different for the γ(111)//α(110) interface (see section 3.4.2.1).

For the present interface, applied loading only has a significant influence on the activation energy of the interface mobility in case of a relatively high random site density *and* in the presence of vacancies, whereas for the γ(111)//α(110) interface applied loading also has such a significant influence when, in absence of vacancies, only the random site density is increased. Apparently, for the γ(11-2)//α(111) interface, in the absence of vacancies the stress-induced difference in local environment of the jumping atoms is too subtle to significantly influence the activation energy of the interface mobility. If no stress is applied or

compressive loading is applied, introducing vacancies increases the activation energy of the interface mobility (cf. intercept values in Table 3.4). This increase is due to the formation of clusters of occupied random sites around vacancies at the interface (see discussion in section 3.4.2.1).

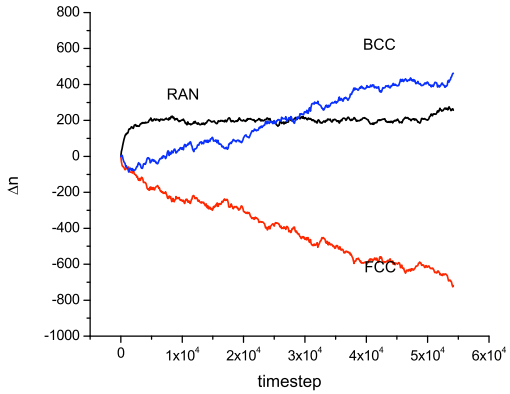

Figure 3.9: The difference in number of occupied sites, Δn, at specific time steps plotted for each type of site (BCC= α sites; FCC = γ sites; RAN = random sites) over the course of a simulation for a typical successful transformation for the $\gamma(11\bar{2})//\alpha(111)$ interface with no applied stress, with five vacancies inserted in the γ interface layer, and with ten random sites per simulation cell at 2028 K.

Strikingly, in the presence of vacancies the activation energy of the interface mobility for the $\gamma(111)//\alpha(110)$ interface increases with applied stress (Fig. 3.5), whereas for the γ(11-2)//$\alpha(111)$ interface it decreases with applied stress (Fig. 3.8). This can be understood as follows. As mentioned in section 3.4.2.1, compressive loading has two antagonistic effects: decreasing planar number density in the plane of growth and decreasing free volume per atom. For the

$\gamma(111)//\alpha(110)$ interface with its lateral growth, the former effect is relatively dominant. For the γ(11-2)//$\alpha(111)$ interface the movement of clusters and the growth direction of ferrite is not confined to directions normal to the applied load (cf. Fig. 3.7). Then the change in free volume per atom is relatively important. Hence, for the γ(11-2)//$\alpha(111)$ interface ΔG^a decreases with increasing stress, whereas the reverse holds for the $\gamma(111)//\alpha(110)$ interface.

3.5 Conclusion

The kinetics of the massive austenite (γ) to ferrite (α) phase transformation is governed by series of energetically unfavourable jumps of austenite atoms at the γ/α interface, through which the necessary free volume is created to allow the occupation of previously blocked ferrite sites (see discussion of Fig. 3.2 in section 3.4.1).

The simulations performed in the course of this work, for the case of applied stress during the transformation, all show an increase in the jump yield with increasing simulation temperature, which indicates the necessity of series of atomic jumps, comprising at least two energetically unfavourable intermediate stages, to create the free volume for the final jump to an empty α site. Using this picture for the atomic mechanism of the transformation, the different results obtained for the two interfaces studied lead to the following interpretation of the effect of stress on the austenite to ferrite transformation.

The effect of stress on the activation energy of the interface mobility is much more pronounced in the presence of vacancies. Obviously, an applied stress has

a larger consequence for the atomic structure of the interface if more vacancies are present initially.

Vacancies have two opposite effects on the mobility of the transformation front:

- A vacancy is a source of free volume enabling the movement of the boundary by reducing the amount of necessary extra free volume, thus facilitating the transformation.
- A vacancy at the phase boundary can relax the atomic arrangement of the γ/α interface by the occupation of random sites around the vacancy. *Such relaxed clusters of atoms surrounding a vacancy exert a pinning force on the boundary, thus hindering the transformation*.

The effect of an applied stress perpendicular to the original ferrite/austenite interface depends on the general growth direction of the ferrite phase at the ferrite/austenite phase boundary, which is interface specific:

(i) If the direction of growth is normal to the stress (lateral growth), as for the $\gamma(111)//\alpha(110)$ interface, then a compressive load has two antagonistic effects on the mobility of the transformation front:

  - The free volume per atom decreases, thus hindering the transformation.
  - The planar atomic number density in the plane of (lateral) growth decreases, thus facilitating the transformation.

  As the compressive loading facilitated the transformation in case of lateral

growth it can be concluded that the transformation promoting decreased planar atomic number density predominates the transformation obstructing decrease in free volume per atom. This finding is compatible with the experimental results reported in Ref. [11], where it was shown that compressive loading promotes progress of the transformation in directions normal to the applied stress.

Generally a more "open" structure of the interface (more free volume) will lead to a lower activation energy for the the interface mobility (cf. Figs. 3.4-3.8. at zero stress). However, in case of planar growth, application of tensile stress perpendicular to the plane of growth increases the free volume per atom, but yet the activation energy increases as a consequence of an increase of the atomic number planar density.

(ii) If the growth mode is (more) isotropic, as for the γ(11-2)//α(111) interface, the planar atomic density does not govern the transformation kinetics. Instead, the stress-induced change in free volume per atom controls the dependence of the activation energy on applied stress: the activation energy decreases with increasing stress (compressive $\rightarrow$ tensile).

Acknowledgements

One of the authors (MB) would like to thank the German Research Foundation (DFG) for financial support of the project within the Cluster of Excellence in Simulation Technology (EXC 310/1) at the University of Stuttgart.

REFERENCES

[1] J. W. Christian. *The Theory of Transformations in Metals and Alloys*. Pergamon Press, Oxford, 2002.

[2] E. J. Mittemeijer. *Fundementals of Materials Science*. Springer-Verlag Berlin Heidelberg, 2010.

[3] T. Massalski, *Metall. Mater. Trans. A*, 33(8):2277–2283, 2002.

[4] H. I. Aaronson, *Metall. Mater. Trans. A*, 33(8):2285–2297, 2002.

[5] H. I. Aaronson and V. Vasudevan, *Metall. Mater. Trans. A*, 33:2445–2470, 2002.

[6] Y. Liu, F. Sommer, and E. J. Mittemeijer, *Acta Mater.*, 51(2):507 – 519, 2003.

[7] Y. Liu, F. Sommer, and E. J. Mittemeijer, *Acta Mater.*, 52(9):2549 – 2560, 2004.

[8] Y. Liu, F. Sommer, and E. J. Mittemeijer, *Acta Mater.*, 54(12):3383 – 3393, 2006.

[9] G. Mohapatra, F. Sommer, and E. J. Mittemeijer, *Acta Mater.*, 55(13):4359 – 4368, 2007.

[10] Y. Liu, D. Wang, F. Sommer, and E. J. Mittemeijer, *Acta Mater.*, 56(15):3833 – 3842, 2008.

[11] Y. Liu, F. Sommer, and E. J. Mittemeijer, *Acta Mater.*, 57(9):2858 – 2868, 2009.

[12] C. Bos, J. Sietsma, and B. J. Thijsse, *Phys. Rev. B*, 73:104117–104124, 2006.

[13] S. Tateyama, Y. Shibuta, and T. Suzuki, *ISIJ Int.*, 50(8):1211–1216, 2010.

[14] S. Tateyama, Y. Shibuta, T. Kumagai, and T. Suzuki, *ISIJ Int.*, 51(10):1710–1716, 2011.

[15] H. Song and J. Hoyt, *Acta Mater.*, 60(10):4328 – 4335, 2012.

[16] C. Bos, F. Sommer, and E. J. Mittemeijer, *Acta Mater.*, 52(12):3545 – 3554, 2004.

[17] C. Bos, F. Sommer, and E. J. Mittemeijer, *Acta Mater.*, 53(20):5333 – 5341, 2005.

[18] C. Bos, F. Sommer, and E. J. Mittemeijer, *Model. Sim. Mater. Sc. Eng.*,

14(2):273–282, 2006.
[19] C. Bos, F. Sommer, and E. J. Mittemeijer, *Philos. Mag.*, 87(16):2245–2262, 2007.
[20] M. S. Daw and M. I. Baskes, *Phys. Rev. Lett.*, 50(17):1285–1288, 1983.
[21] M. S. Daw and M. I. Baskes, *Phys. Rev. B*, 29(12):6443–6453, 1984.
[22] R. A. Johnson and D. J. Oh, *J. Mater. Res.*, 4(5):1195–1201, 1989.
[23] M. Kaukonen, J. Peräjoki, R. M. Nieminen, G. Jungnickel, and T. Frauenheim, *Phys. Rev. B*, 61(2):980–987, 2000.
[24] R. Fletcher and C. M. Reeves, *Comput. J.*, 7(2):149–154, 1964.
[25] K. A. Fichthorn and W. H. Weinberg, *J. Chem. Phys.*, 95(2):1090–1096, 1991.

Chapter 4

Mobility of the austenite-ferrite interface under various states of loading

M. Biglari Jr. and E.J. Mittemeijer

Abstract

The massive austenite-ferrite phase transformation was simulated on an atomic scale for various states of loading: uniaxial, planar and hydrostatic. The simulated system involved the lateral growth of a two-dimensional ferrite seed at the ferrite-austenite phase boundary for a variable number of vacancies at the interface. The atomistic simulation was based on application of a recently developed multi-lattice kinetic Monte Carlo method. The effects of the different states of loading and of the vacancy concentration at the interface were discussed in terms of their impact on the necessary local rearrangement of austenite atoms to unblock unoccupied ferrite-lattice sites. It followed that the net outcome of the effects of additional free volume and of vacancy pinning strongly depends on the state of loading.

4.1 Introduction

Solid state phase transformations are an important means to change/control the microstructure of materials and therewith the properties of workpieces consisting of those materials[1, 2]. The massive solid state phase transformation from austenite (γ) to ferrite (α) in iron-based alloys and steels is certainly one of the technologically most important phase transformations[3]. This transformation exhibits nucleation and growth modes of complex nature[4–6]. The formation of the product phase is achieved by local rearrangements of the atoms at the phase boundary, in the absence of long-range diffusion of the reacting species[3, 7, 8]. The atomic mechanisms involved in this transformation cannot be revealed by experimental methods, as the transformation is completed within a few seconds at elevated temperatures. Therefore atomistic simulations appear to have great potential to shed light on the fundamentals of the kinetics of this transformation.

During production and usage of iron-based alloys and steels the components can be subjected to pronounced stresses. It has been experimentally established that residual stresses and applied, external loads have a significant influence on the massive austenite-ferrite transformation in iron and steels[9, 10]. In the present project the focus is on the role of applied stress on the massive $\gamma \rightarrow \alpha$ phase transformation by atomic simulations. First attention was paid to the nucleation mode[11]. Now we turn to the growth kinetics under various different states of applied stress.

Atomistic simulations may be performed employing Molecular Dynamics

(MD) methods[12–16]. However, as observed by Tateyama et al.[13] results obtained by such simulations are strongly dependent on the choice of the interatomic potential. The application of Molecular Dynamics (MD)methods for simulation of the phase transformation kinetics is not advisable in the present case: a driving force for the transformation (which is given by the employed potential) should be selected that is neither so high that the martensitic transformation prevails[7] nor so low that the massive transformation cannot take place within MD time scales[17]. Moreover, the investigation of the effects of stress on the austenite-ferrite interface mobility requires large numbers of simulations, to obtain enough data to reveal statistically assured results for the different states of stress(see section 4.2), so that MD is infeasible due to its computational cost. Therefore, the atomistic simulations in this project were performed with the kinetic Monte Carlo method. This method, which requires much lower computational cost, allows inherently non-coordinated movement of atoms and covers much longer time scales and thus is more suited to simulate the mobility of the austenite-ferrite interface. This has been demonstrated in previous work, where the basis of this method, in the absence of applied stress, was developed[8, 17]. The present paper presents a comparative investigation of the influence of different states of loading (uniaxial, planar (rotationally symmetric) and hydrostatic states of stress) on the mobility of the α/γ interface.

4.2 Simulation Method

The basics for application of the kinetic Monte Carlo Method to a multilattice system for the transformation of austenite to ferrite has been presented in Refs. [8, 17]. Its extension to running the transformation subjected to more general state of stress is straightforward. The essentials of the simulation method, necessary for understanding of this paper, are presented below.

The atoms are distributed over discrete sites in space. These discrete sites are given by the crystal lattices of austenite and ferrite crystal blocks in specific orientations and randomly dispersed sites. These random sites can be occupied to provide realistic descriptions of irregular, austenite-ferrite interface structures. During the course of a simulation, atoms jump from an occupied site to an empty site. The following basic simulation loop is employed:

(1) Create a list of interface atoms. An atom is on a so-called interface site if it is next to an atom of different type or next to a vacancy. A jump to an empty site is in principle possible if the empty site is within a predefined range from the interface atom and if that empty site itself is not too close to another atom.

(2) Determine all possible jumps for each interface atom to neighbouring empty sites.

(3) Calculate the jump rate, k_i for each jump i according to $k_i = \nu_0 \exp[-E_i^a / k_b T]$, where E_i^a is the activation energy for a single atomic jump, ν_0 is a frequency factor and k_b is the Boltzmann constant and T is the temperature.

(4) Calculate the total jump rate $K_{\mathrm{sum}} = \sum_i^N k_i$, where N is the total number of jumps.

(5) Determine a random number R_1 between 0 and K_{sum}.

(6) The first jump a with $\sum_i^a k_i > R_1$ is selected and executed.

(7) Determine the elapsed real time Δt with a second random number R_2 according to [18] $\Delta t = \frac{\ln(R_2)}{K_{sum}}$.

(8) Add Δt to the time t and the time step (i.e. the number of jumps made) is increased by one.

(9) Continue with step 1.

The activation energy of a single atomic jump can in principle be calculated by the Locally Activated Monte Carlo Method as presented in Ref. [19] and calculating the cohesive energy for a certain atomic configuration by using the Embedded Atom Method[20, 21] with the potential developed by Johnson and Oh[22].

Calculating the activation energy in this manner for each individual jump during the simulation would retard the simulation much too much. Therefore a neural network was trained on a basis set of 35000 individual jumps in a system under no applied stress. For each jump the rigorously calculated activation energy for the single atomic jump (as described above) was stored as output parameter with, as input parameters, the difference in cohesive energy before and after the jump, the jump distance and the distance of the fourteen nearest neighbours. Using validation sets obtained for the systems under different amounts of

stress, the mean square error for the activation energy for a single atomic jump was found to be less than 8% in all cases.

After 50000 jumps unused random sites were redistributed and the austenite crystal block was moved in the direction normal to the interface to accommodate the volume misfit between the austenite and ferrite phases. The simulation was ended after ten million jumps or after a certain number of one type of sites had become occupied (see below).

This method was used here to simulate the lateral growth of a two-dimensional ferrite nucleus at the ferrite/austenite interface subjected to a specified state of stress. This was done by creating a bicrystal with a flat interface by taking (strained) crystal blocks of each phase and joining them according to the $\gamma(111)//\alpha(110)$; $\gamma[11\bar{2}]//\alpha[001]$ Orientation Relationship. The direction normal to the interface in the direction of the austenite is the positive z-direction. In the austenite interface layer a rectangular ferrite nucleus was inserted in the middle along the x-direction (cf. Fig. 4.1). Vacancies were added by randomly removing eleven austenite atoms from the interface. The random sites were distributed according a restricted random distribution: the system was divided in cells with edges slightly larger than the austenite next nearest neighbour distance and a certain number of random sites was distributed randomly in each cell. The higher the number of random sites, the more computation time is spent on for the transformation irrelevant jumps of atoms back and forth between crystal lattice sites and random sites very near to them. However, reducing the number of random sites too much obstructs expressing well the differences between different states of stress, as too few opportunities occur for realising different

interface structures. The number of random sites per cell in this work was five for all simulations, which was shown to be a good compromise between computational efficiency and variable interface structure. Simulations were set to finish when the number of occupied ferrite sites had increased with a number equal to 80% of the number of remaining austenite atoms in the interface layer. During simulations periodic boundary conditions in the *x*- and *y*-directions are maintained, while atoms in the two layers at the top of the system and the two layers at the bottom of the system were not considered as interface atoms.

The strains in the crystals blocks caused by a state of stress were calculated separately for each phase by solving for the strains the following three equations for a cube in an infinite, perfect crystal orientated to *xyz* in accordance with the crystallographic OR (see above):

$$\frac{\partial E_{\text{coh}}}{L\partial\varepsilon_x} = -F_x, \frac{\partial E_{\text{coh}}}{L\partial\varepsilon_y} = -F_y \text{ and } \frac{\partial E_{\text{coh}}}{L\partial\varepsilon_z} = -F_z \tag{4.1}$$

where E_{coh} is the cohesive energy of the cube, L is the initial edge length of the cube, F_j is the force applied to the cube in direction j and ε_j is the strain in direction j. The uniaxial state of stress was applied normal to the interface plane: $F_x = F_y = 0, F_z$; the bi-axial, rotationally symmetric planar state of stress was applied in the interface plane with equal applied forces (stresses) in the x and y directions: $F_x = F_y, F_z = 0$; and the hydrostatic state of stress was applied by imposition of equal forces (stresses) along the x, y and z directions: $F_x = F_y = F_z$. For each state of stress the values of the principal stress components were varied from -1600 MPa to 1600 MPa in steps of 400 MPa.

Simulations were performed for five equidistant temperatures between 2028 K and 3042 K. As in this simulation method the atoms have no impulse, the temperature only influences the jump rates (i.e. the transformation kinetics) and not the energy difference of ferrite and austenite (i.e. the thermodynamic driving force), and therefore these high temperatures can and should be employed for enhancing the computational efficiency (see also Refs. [8, 17]).

For a specific system as defined by an austenite-ferrite OR, amount of vacancies, random site density, temperature and a specific state of stress, the simulation was repeated 48 times with the only difference being different seeds for the random numbers and the initial distribution of random sites, in order to obtain a statistically assured result for the transformation rate in the case considered.

The transformation rate, r_{tf}, (the number of net jumps towards α lattice sites divided by the corresponding time lapsed) was determined each time after 400 atoms had transformed. The transformation rates, r_{tf}, obtained for the 240(=5x48) simulations for the five different temperatures were fitted non-linearly as function of the temperature, T, according to[1, 2]

$$r_{tf}(T) = \underbrace{M_0 \exp\frac{-\Delta G^a}{k_b T}}_{\text{M=interface mobility}} \left(1 - \exp\left(-\frac{|\Delta U_{\mathrm{fcc,bcc}}|}{k_b T}\right)\right), \tag{4.2}$$

where M_0 is a pre-exponential factor, ΔG^a is the activation energy for the transformation and $\Delta U_{\mathrm{fcc,bcc}}$ is the driving force of the reaction; M_0 and ΔG^a are the fitted parameters.

4.3 Results and Discussion

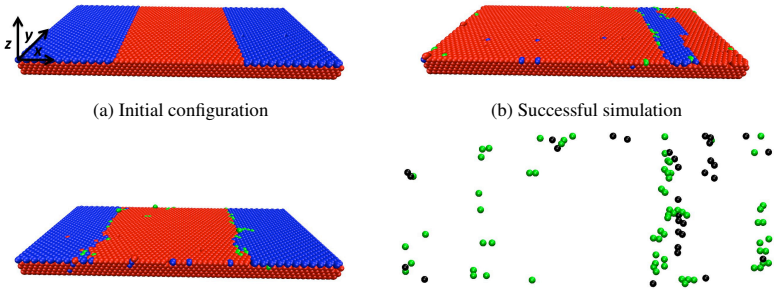

(a) Initial configuration

(b) Successful simulation

(c) Unsuccessful simulation

(d) Random sites

Figure 4.1: The $\gamma(111)//\alpha(110)$; $\gamma[11\bar{2}]//\alpha[001]$ system before (a) and after (b, c) simulation, with α atoms represented by red spheres, γ atoms by blue spheres and atoms at random sites with green/black spheres. The γ atoms above the interface layer are not shown to realize a clearer overview. The final state of simulations was either a (full) transformation of the layer (successful transformation) (b) or an interface where the initial interface has moved little and atoms mainly jumped to random sites (unsuccessful transformation) (c). In a top view only showing occupied random sites for the successful and unsuccessful transformation (d) reveals that for the unsuccessful transformation (green spheres) there are more random sites occupied than for the successful transformation (black spheres).

Two types of end results were observed, either a transformation of the austenite layer, at the interface of the crystal blocks, to ferrite (i.e. the simulation was successful) accompanied with an increase in occupied random sites (cf. Fig. 4.1(b)) or the simulation was unsuccessful accompanied with, as compared to a successful transformation, a relatively larger increase in the number of occupied random sites along the γ/α interface boundary (between the ferrite nucleus and the remaining part of the austenite layer adjacent to the interface of the α and γ crystal blocks) with little or no (net) movement of that interface boundary (cf.

Fig.4.1(c)). These two different outcomes are the consequence of the likelihood of simulation leading to a specific end configuration. Principally a simulation can lead to every configuration where the number of atoms on ferrite sites is equal to or lower than the number which stops the simulation. The chance that a particular end configuration occurs, depends on the number of pathways to such an end configuration and the chance that such a pathway is taken. The chance for successful transformation depends on the likelihood of sequences of jumps (pathways) being picked which lead to net movement of the boundary, whereas sequences of jumps between only crystal lattice sites and random sites do not promote the transformation. Both types of pathway, once chosen, experience reinforcement, i.e. the success of a simulation is determined to a large part by the initial stage of the simulation. For more background on this dichotomy, see Ref. [23].

For all states of stress considered, the number of successful simulations increased with increasing temperature. This can be understood as consequence of the observed increase in the jump yield for higher temperatures, which indicates that the transformation is realized by sequences of atomic jumps involving at least two energetically unfavourable intermediate stages (see Appendix B in Ref. [8]): the $\gamma \rightarrow \alpha$ transformation proceeds via local rearrangement of the atoms on austenite sites to create the necessary free volume around unoccupied ferrite sites (see Fig. 4.2).

In case of uniaxial loading, the number of successful runs increases when the applied stress (algebraically) increases from compressive to tensile. For bi-axial loading the reverse holds, while the for the case of a hydrostatic state of stress

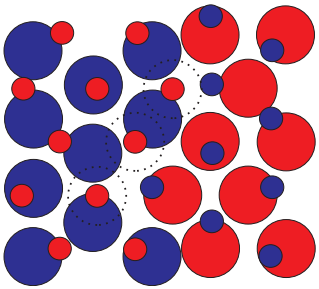

Figure 4.2: Zoomed on schematic top view of the austenite-ferrite interface layer with the occupied and unoccupied crystal sites shown simultaneously. The α atoms and sites have been represented by red spheres, γ atoms and sites by blue spheres. Occupied sites are shown by larger spheres and unoccupied sites are shown by smaller spheres. The dotted lines around several of the empty ferrite sites serve to show that occupation of that site by an atom on one of the neighbouring austenite sites would lead to large overlap with the other occupied austenite sites, thereby illustrating the necessity of local atomic rearrangement prior to occupation of such a ferrite site.

no such trend can be discerned (see Fig. 4.3). This can be understood as follows. The necessary (local) rearrangements to realise the $\gamma \rightarrow \alpha$ transformation (see Fig. 4.2) can be achieved by *in-plane* rearrangements, where the γ atoms blocking unoccupied α sites jump to random sites on roughly the same height as the transformation plane, or by the more common *out-of-plane* rearrangements, where the γ atoms jump to random sites at heights (z values) distinctly different from that of the transformation plane. The less common in-plane rearrangement will become more likely upon uniaxial compressive loading and upon bi-axial tensile loading, as the planar number density in the plane of growth will decrease, while the distances between the lattice planes parallel to the original interface between the α and γ crystal blocks is decreased. Similarly, the more

common out-of-plane rearrangement will become (even) more likely upon uni-axial tensile loading and upon bi-axial compressive loading.

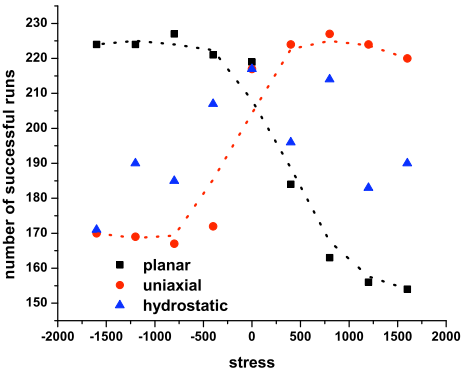

Figure 4.3: The number of successful simulation runs, on a total of 240 runs, as function of applied principal stress component(s) for the $\gamma \rightarrow \alpha$ transformation at the $\gamma(111)//\alpha(110)$ interface with 11 vacancies inserted in the γ interface layer and five random sites per simulation cell for uniaxial, planar and hydrostatic states of stress. Moving average lines have been drawn to guide the eye.

The overall dependence of the number of successful runs on the value of the principal stress component(s) in case of uniaxial loading and biaxial loading and the lack of such an overall dependence for the case of hydrostatic loading reveal that the observed trend for uniaxial and bi-axial loading is caused by the tetragonal distortion induced by the state of stress rather than the associated change in free volume. This can be explained by looking to the change in jump rates k_i for the individual atomic jumps. In the case of uniaxial or bi-axial stress the change in k_i for a specific jump in the unstressed state as compared to the

stressed state depends on the jump direction. In the case of hydrostatical stress the change in k_i for all jumps upon applying stress is roughly the same, and thus, in this case, little or no clear influence can be expected from the application of stress within the investigated range.

4.3.1 The Activation Energy, ΔG^a

An exemplary result of fitting of Eq. 4.2 to the data for the transformation rate as obtained from 240 different simulations is shown in Fig. 4.4 for the case of applied biaxial, rotationally symmetric, planar stress, with $\sigma \equiv \sigma_{xx} = \sigma_{yy} = -1600$ MPa and with 11 vacancies in the transformation layer. The error bars shown represent the standard deviations of the obtained values for the transformation rate (at a fixed temperature) to illustrate the necessity for a lot of repetitions of the same simulation (with different seeds for the random numbers and initial distribution of the random sites) to obtain a statistically assured average value for the transformation rate (cf. section 4.2). Such fits were performed for values in the range considered for the principal applied stress components and for certain numbers of random sites per simulation cell and of vacancies in the transformation layer. The results obtained for the activation energy of the interface mobility, ΔG^a, as function of the principal applied stress components, with five random sites per simulation cell and 11 vacancies at the transformation layer, are shown in Fig. 4.5 for uniaxial, planar and hydrostatic states of stress. To investigate the trend of the activation energy of the interface mobility as function of principal applied stress component a linear fit to the data for ΔG^a as function of principal stress component was made for each state of stress. As

linear fits are sensitive to outliers, each fit was repeated leaving out the point with the largest residual. If the slope and the intercept were equal for both fits within the standard error, the results of the fit were accepted. For all cases considered in this work no such outliers could be identified. The results of the linear fits for all simulations are presented in Table 4.1.

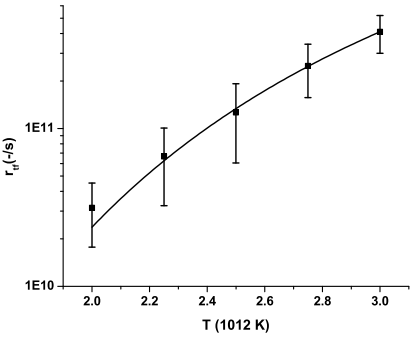

Figure 4.4: The transformation rate, r_{tf}, as function of temperature. The results have been obtained for simulations for the $\gamma(111)//\alpha(110)$ system with five random sites per simulation cell, an applied planar, rotationally symmetric state of stress with $\sigma \equiv \sigma_{xx} = \sigma_{yy} = -1600$ MPa, and with 11 vacancies inserted in the transformation layer. The data points represent the average transformation rates and the error bars represent the standard deviation. The line drawn has been obtained by non-linear least-squares fitting of Eq. (4.2) to the data points for the transformation rate as function of temperature.

Vacancies can influence the transformation in two ways:

1. The presence of vacancies lowers the atomic number planar density in the transformation layer, provides extra free volume at the moving interface and thereby lowers the necessary extent of local rearrangement to establish

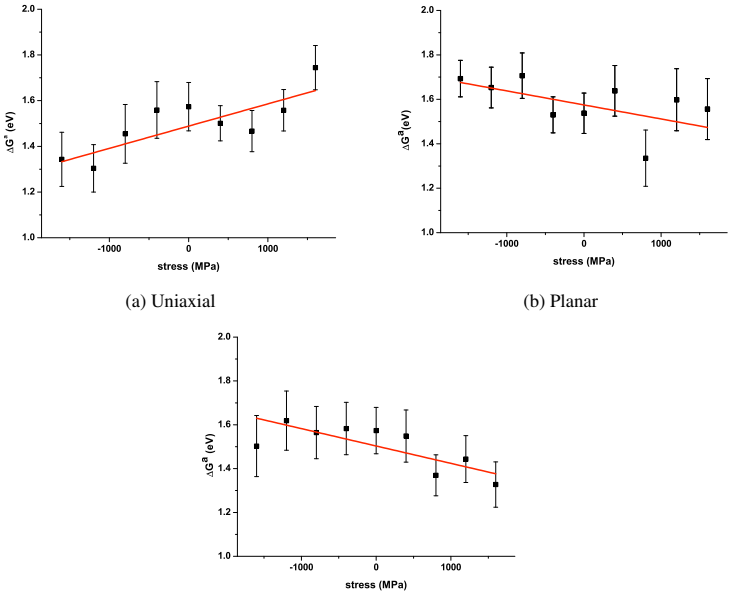

(a) Uniaxial

(b) Planar

(c) Hydrostatic

Figure 4.5: The activation energy of the interface mobility, ΔG^a, as function of applied principal stress component(s). The results have been obtained from simulations for the $\gamma(111)//\alpha(110)$ system with five random sites per simulation cell and with 11 vacancies inserted in the transformation layer. The data points are the results of non-linear least-squares fitting of Eq. (4.2) to the transformation rates obtained from simulations as function of temperature (as in Fig. 4.4). The error bars assigned to the data points indicate the standard error for the non-linear fit of Eq. (4.2). The straight lines drawn represent linear fits to the data points in the figure (see text).

progress of the transformation. This effect contributes to a decrease of the activation energy of the interface mobility.

2. The transformation interface can be pinned by a vacancy as the stress field surrounding a vacancy can be partly relaxed by atoms occupying random

Table 4.1: Results obtained for the straight line fitted to the data points obtained for the activation energy of the interface mobility, ΔG^a, as function of applied principal stress component(s) for the $\gamma(111)//\alpha(110)$ system. "Vac" designates the number of vacancies inserted in the transformation layer; "Slope" and "SE slope" represent the slope of the fitted straight line and its standard error; "Intercept" and "SE intercept" correspond with the intercept of the fitted straight line with the ordinate at zero stress and its standard error ($\sigma \equiv \sigma_{zz}$ in case of uniaxial loading; $\sigma \equiv \sigma_{xx} = \sigma_{yy}$ in the case of biaxial loading; $\sigma \equiv \sigma_{xx} = \sigma_{yy} = \sigma_{zz}$ in the case of hydrostatic loading).

State of stress	Vac	Slope (eV/MPa)	SE Slope (eV/MPa)	Intercept ($\sigma = 0$) (eV)	SE Intercept (eV)
Uniaxial	0	4.3e-5	3.9e-5	1.51	0.04
Uniaxial	11	9.7e-5	3.4e-5	1.49	0.03
Planar	0	-1.3e-5	4.5e-5	1.52	0.05
Planar	11	-6.3e-5	3.5e-5	1.57	0.04
Hydrostatic	0	-1.5e-4	4.5e-5	1.48	0.05
Hydrostatic	11	-7.9e-5	3.8e-5	1.50	0.04

sites neighbouring the vacancy. To move such a vacancy from such a relaxed region or to transform the region around requires a relative large extent of local rearrangement (see Fig. 4.6). This contributes to an increase of the activation energy of the interface mobility.

In the stress-free condition the introduction of vacancies at the transformation layer does not significantly* influence the activation energy of the interface mobility (see intercept values (at $\sigma = 0$) in Table 4.1). Evidently, when no stress is applied the above discussed effects (i) and (ii) cancel each other out.

In the absence of vacancies at the austenite-ferrite interface, in the case of

*In this work a difference is considered to be significant if the null hypothesis[24] can be rejected with more than 95% confidence.

planar or uniaxial states of stress the activation energy does not change significantly as function of the principal stress component(s), whereas in the case of a hydrostatic state of stress the activation energy increases significantly as the applied stress goes from tensile to compressive (cf. Table 4.1). This can be discussed as follows.

By applying uniaxial compression (normal to the interface plane) or bi-axial tension (in the plane of growth) it holds:

(a) the planar number density in the plane of growth decreases, and

(b) the lattice-plane spacing of the planes parallel to the interface of the ferrite and austenite crystal blocks decreases.

With a view to the occurring planar growth mode, the first effect (a) facilitates the transformation, as less local rearrangement is required before empty ferrite sites become available for occupation, whereas the second effect (b) suppresses the transformation. Of course, effects (a) and (b) are of opposite nature if the applied states of stress are uniaxial tension and biaxial compression. Evidently, in the absence of vacancies, in case of a uniaxial or a planar state of stress, the net outcomes of the combined effects (a) and (b) are that small that no significant changes of the activation energy of the interface mobility can be observed as function of the principal stress component(s). However, as compared to the cases of uniaxial compression and biaxial tension, in case of hydrostatic compression effect (b) is similar, but effect (a) is reversed, implying that in this case both effects suppress the transformation and ,indeed, the largest value for the slope of ΔG^a as function of applied stress occurs for a state of hydrostatic stress

(see Table 4.1).

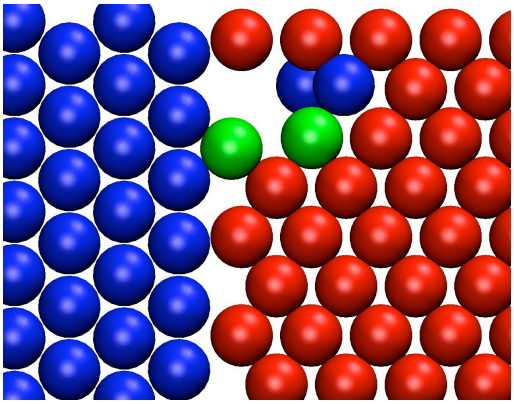

Figure 4.6: Top view of the austenite-ferrite interface layer zoomed on a vacancy at the γ/α interface with its relaxed surrounding atomic configuration. The α atoms have been represented by red spheres, γ atoms by blue spheres and atoms at random sites with green spheres.

Upon introducing vacancies, now the activation energy of the interface mobility does depend on the value of the principal stress component(s) for *all* states of stress. The activation energy of the interface mobility increases significantly for hydrostatic and planar states of stress when the principal stress components change from tensile to compressive value, whereas for uniaxial loading an opposite trend is observed (cf. Table 4.1 and see Fig. 4.5). Experimental evidence supports the above results: uniaxial compression promotes the massive austenite to ferrite transformation, whereas uniaxial tension hinders the massive austenite to ferrite transformation[9, 10]. These effects can be explained as follows.

Vacancies can facilitate the transformation if they are mobile (i.e. not pinned;

see above discussion), so that the free volume associated with the vacancy is available to reduce the necessary extent of local atomic rearrangement. The in-plane mobility of vacancies is obviously increased under uniaxial compression, hydrostatic tension or planar tension, whereas the reverse holds for uniaxial tension, hydrostatic compression or planar compression. So, as compared to the stress-free case where effects (i) and (ii) compensate each other (see discussion above), in the former case effect (i) now dominates, which leads to a decrease of the activation energy of the interface mobility, whereas in the latter case the effect (ii) now dominates, which leads to an increase in the activation energy of the interface mobility (cf. Table 4.1). It is not especially the change in the amount of (excess) free volume, due to the hydrostatic component of the stress field imposed, but, in particular, the anisotropic nature of the imposed deformation, which determines the nature of the change of the activation energy as function of applied stress.

4.4 Conclusions

- The effect of a (state of) applied stress on the mobility of the austenite-ferrite interface depends on the orientation of the principal stress components with respect to the direction of growth of the ferrite phase at the ferrite/austenite phase boundary.
- The kinetics of the transformation in a state of stress, as function of the value of the principal stress component(s), can only be understood recognising the generally anisotropic nature of the deformation induced, rather

than considering (only) the change in (free) volume corresponding to the hydrostatic component of the stress field imposed.

- In the absence of stress, vacancies at the austenite/ferrite interface do not significantly influence the activation energy of the interface mobility: the effect of addition of free volume is compensated more or less fully by the pinning effect caused by relaxation of the atomic configuration surrounding the vacancies.

- In the presence of stress and in the absence of vacancies at the austenite/ferrite interface, only the hydrostatic component of the applied stress field influences significantly the activation energy of the interface mobility, because the stress-induced changes of both the planar number density in the plane of growth and the lattice-plane spacing of the lattice planes parallel to the plane of growth work in the same direction.

- In the presence of stress and in the presence of vacancies at the austenite-ferrite interface, for increasing principal stress component(s) (compressive $\rightarrow$ tensile) the activation energy of the interface mobility increases for a uniaxial state of stress and decreases for planar and hydrostatic states of stress. These effects are dominated by the degree of mobility of the vacancies in the plane of growth allowed by the imposed specific state of stress.

Acknowledgements

One of the authors (MB) would like to thank the German Research Foundation (DFG) for financial support of the project within the Cluster of Excellence in Simulation Technology (EXC 310/1) at the University of Stuttgart.

REFERENCES

[1] J. W. Christian. *The Theory of Transformations in Metals and Alloys*. Pergamon Press, Oxford, 2002.

[2] E. J. Mittemeijer. *Fundementals of Materials Science*. Springer-Verlag Berlin Heidelberg, 2010.

[3] H. I. Aaronson, *Metall. Mater. Trans. A*, 33(8):2285–2297, 2002.

[4] Y. C. Liu, F. Sommer, and E. J. Mittemeijer, *Philos. Mag.*, 84(18):1853–1876, 2004.

[5] Y. Liu, F. Sommer, and E. J. Mittemeijer, *Acta Mater.*, 52(9):2549 – 2560, 2004.

[6] Y. Liu, F. Sommer, and E. J. Mittemeijer, *Acta Mater.*, 54(12):3383 – 3393, 2006.

[7] T. Massalski, *Metall. Mater. Trans. A*, 33(8):2277–2283, 2002.

[8] C. Bos, F. Sommer, and E. J. Mittemeijer, *Acta Mater.*, 53(20):5333 – 5341, 2005.

[9] Y. Liu, F. Sommer, and E. J. Mittemeijer, *Acta Mater.*, 57(9):2858 – 2868, 2009.

[10] G. Mohapatra, F. Sommer, and E. J. Mittemeijer, *Acta Mater.*, 55(13):4359 – 4368, 2007.

[11] M. Biglari Jr. and E. J. Mittemeijer, *Model. Sim. Mater. Sc. Eng.*, 20(7):075010, 2012.

[12] S. Tateyama, Y. Shibuta, and T. Suzuki, *Scr. Mater.*, 59:971–974, 2008.

[13] S. Tateyama, Y. Shibuta, and T. Suzuki, *ISIJ Int.*, 50(8):1211–1216, 2010.

[14] S. Tateyama, Y. Shibuta, T. Kumagai, and T. Suzuki, *ISIJ Int.*, 51(10):1710–1716, 2011.

[15] H. Song and J. Hoyt, *Acta Mater.*, 60(10):4328 – 4335, 2012.

[16] C. Bos, J. Sietsma, and B. J. Thijsse, *Phys. Rev. B*, 73:104117–104124, 2006.

[17] C. Bos, F. Sommer, and E. J. Mittemeijer, *Acta Mater.*, 52(12):3545 – 3554, 2004.

[18] K. A. Fichthorn and W. H. Weinberg, *J. Chem. Phys.*, 95(2):1090–1096, 1991.

[19] M. Kaukonen, J. Peräjoki, R. M. Nieminen, G. Jungnickel, and T. Frauenheim, *Phys. Rev. B*, 61(2):980–987, 2000.
[20] M. S. Daw and M. I. Baskes, *Phys. Rev. Lett.*, 50(17):1285–1288, 1983.
[21] M. S. Daw and M. I. Baskes, *Phys. Rev. B*, 29(12):6443–6453, 1984.
[22] R. A. Johnson and D. J. Oh, *J. Mater. Res.*, 4(5):1195–1201, 1989.
[23] M. Biglari Jr. and E. J. Mittemeijer, *Submitted for Publication*, 2012.
[24] E. Lehmann and J. P. Romano. *Testing Statistical Hypotheses*. Springer New York, 2005.

Chapter 5

Summary

5.1 English summary

In the thesis the effects of applied stress on the massive transformation on an atomic scale was investigated by Molecular Statics and Monte Carlo methods.

5.1.1 Energetics of nucleation at the austenite-ferrite interface

Two-dimensional nucleation has been suggested as a mechanism for ledge generation for the ledge-wise growth of the massive phase [1, 2]. To investigate the effects of applied uniaxial loading on the two-dimensional nucleation of ferrite at an originally flat austenite-ferrite interface, Molecular Statics simulations have been performed. The cohesive energy for a bicrystal with a circular ferrite seed with a thickness of one, five or ten atomic layers and a radius r at a flat interface (with a bcc(110)//fcc(111); bcc[001]//fcc[11-2]-interface orientation) under uniaxial stress, σ, applied along the direction normal to the flat interface orientation was minimised. The cohesive energy can be fitted as function of the radius, r, with the interface energy, γ, and the misfit-strain energy per unit

volume transformed, C, as fitting parameters.

The interface energy decreased for increasing applied tensile stress, because of an increasing distance between austenite and ferrite atoms at the circumference of the interface, thus the repulsion between these ferrite and austenite atoms is decreased (cf. Fig. 5.1a). For increasing compressive applied stress the interface energy reached a plateau due to a minimal distance between atoms imposed by the simulation method. With increasing nucleus thickness the interface energy increases, because the relative importance of the favourable interaction between austenite atoms at the top layer and favourable interaction between ferrite atoms at the bottom layer of the nucleus decreases.

Using continuum approaches [3, 4] the misfit strain energy can be calculated as consequence of the volumetric misfit as given by the difference in density between ferrite and austenite. These continuum approaches fail to predict misfit strain energy, C, obtained by the simulations for particles in the size range considered in this work (cf. Fig. 5.1b). This is ascribed to the presence of excess free volume at the interface, which cannot be neglected with the high surface to volume ratio for such small particles. Using the simulation obtained misfit strain energy and interface energy, the dependencies of the critical radius for nucleation, r_c , and the associated energy of nucleus formation, ΔG^*, on applied stress can be established.

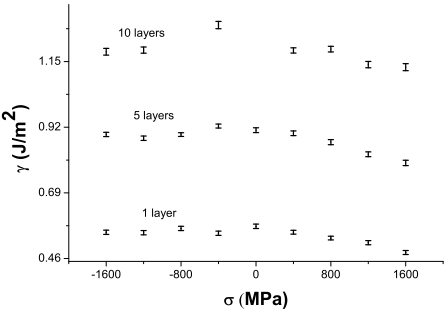

(a) γ

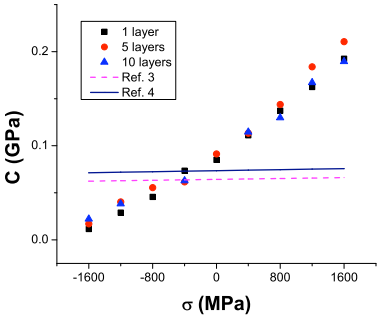

(b) C

Figure 5.1: The interface energy, γ (a), and the misfit-strain energy, C (b), as function of applied stress σ. Results obtained by fitting to the simulated data points. The error bars represent the standard error for the fit. The predicted values of C, also shown in (b) (note C in principle depends on σ), have been obtained according to the continuum physics approaches presented in Refs. [3] and [4].

5.2 Massive austenite-ferrite transformation under loading

The growth of ferrite at the ferrite/austenite interface at atomic time and length scales has been simulated by means of multi-lattice kinetic Monte Carlo [5, 6]. The investigated systems were bicrystals with a two-dimensional ferrite seed at the ferrite-austenite interface. Simulations have been performed with different crystallographic Orientation Relationships between ferrite and austenite, different state of stress, random site concentration and number of vacancies at the interfaces. Using the simulation obtained transformation rate the activation energy for the interface mobility, ΔG^a, could be established for the considered cases.

First the case of uniaxial loading was investigated for two different interface orientations. It was observed that in the case of $\gamma(11\bar{2})//\alpha(111)$ interface orientation the growth was more isotropic, while for the $\gamma(111)//\alpha(110)$ interface a lateral growth (normal to the direction of loading) of ferrite could be observed. The rate of the massive austenite (γ) to ferrite (α) phase transformation is governed by series of energetically unfavourable jumps of austenite atoms at the γ/α interface, as local rearrangement is necessary to move austenite atoms away and unblock empty ferrite sites. In absence of vacancies for none of the investigated OR, uniaxial loading had a significant effect on the activation energy for the interface mobility. Vacancies were able to enhance the reaction, if the vacancy associated free volume was available, but could suppress the transformation by pinning the interface, if advanced degrees of relaxation took place. In case of anisotropic growth the uniaxial compression enhances

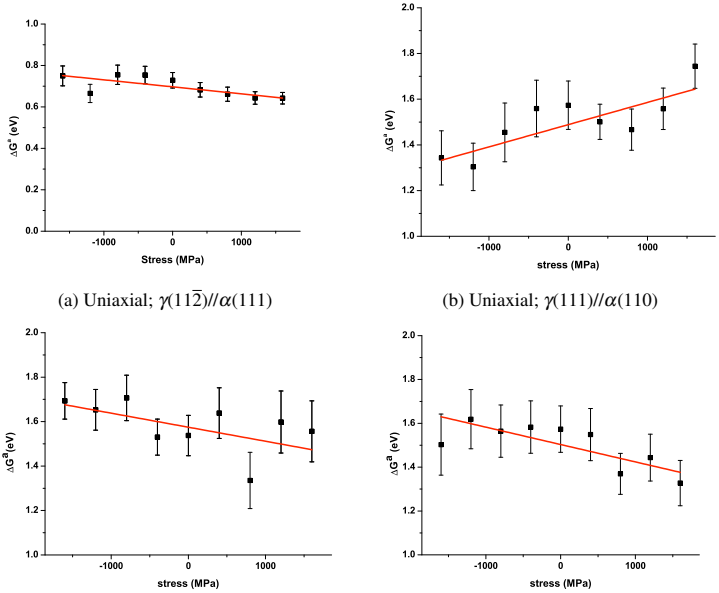

(a) Uniaxial; $\gamma(11\bar{2})//\alpha(111)$

(b) Uniaxial; $\gamma(111)//\alpha(110)$

(c) Planar; $\gamma(111)//\alpha(110)$

(d) Hydrostatic; $\gamma(111)//\alpha(110)$

Figure 5.2: The activation energy of the interface mobility, ΔG^a, as function of applied principal stress component. The results are based on simulations for the $\gamma(111)//\alpha(110)$ system (b, c and d) with five random sites per simulation cell and with 11 vacancies inserted in the transformation layer. The data points and error bars are the results and the standard error of non-linear least-squares fitting the transformation rates obtained from simulations as function of temperature. The straight lines drawn represent linear fits to the data points in the figure.

the reaction as the in-plane mobility of the vacancy increased, due to decreasing planar atomic number density. In case of isostropic growth uniaxial tension enhances the transformation due to an increase free volume per atom.

The case of $\gamma(111)//\alpha(110);\gamma[11\bar{2}]//\alpha[001]$ has also been simulated for a planar state of stress and for a hydrostatic state of stress. The planar state of stress was applied in the plane of growth. It was observed that in absence of vacancies, the activation energy for the interface mobility did not vary significantly in case of a planar state of stress as was the case for a uniaxial state of stress. This can be explained by the observation that for the case of uniaxial tension and planar compression, there is an increase in lattice-plane spacing, which facilitates the transformation, and an increase planar atomic number density, which suppresses the transformation. The net outcome is that in absence of vacancies at the interface no significant influence on the activation energy for the interface mobility can be observed.

However, applied hydrostatic compression increased the activation energy for the interface mobility and hydrostatic tension decreased it. For a hydrostatic compression both the planar atomic nuber density and and the lattic-plane spacing change in a way that suppresses the transformation, while for hydrostatic tension these effcts work in unison to facilitate the transformation. Hence a significant effect on the activation energy could be seen for a hydrostatic state of stress.

For hydrostatic and planar tension and uniaxial compression the transformation is facilitated in presence of vacancies (cf. Figs. 5.2b-d). The common effect in these cases is the decrease of planar atomic number density in the

plane of growth. As stated above the vacancies become mobile as the planar atomic number density is decreased and hence the vacancy-associated free volume becomes available to facilitate the transformation. For hydrostatic and planar compression and uniaxial tension, the reverse holds and there is an increase in planar number density in the plane of growth and the pinning force of the vacancy on the moving interface becomes more significant, hence a suppresion of the transformation can be observed.

5.3 Deutsche Kurzfassung

In dieser Doktorarbeit wurde der Einfluß einer aufgebrachten Spannung auf die massiven Umwandelung mit Hilfe von Molekular Statik (MS) und kinetischen Monte-Carlo-Methoden (kMC) untersucht.

5.3.1 Keimbildungsenergie an der Austenit/Ferrit-Grenzfläche.

Zweidimensionale Keimbildung wurde als ein Mechanismus für die Stufenbildung der massiven Umwandlung vorgeschlagen [1, 2]. Um die Effekte einer angelegten einachsigen Spannung auf die zweidimensionale Ferritkeimbildung an der Austenit-Ferrit Grenzfläche zu ermitteln, wurden MS-Simulationen durchgeführt. Die Bindungsenergie von Bikristallsystemen mit einem kreisförmigen Ferritkeim mit einer Dicke von ein, fünf oder zehn Atomlagen an der Austenit-Ferrit Grenzfläche (Orientierung kfz(110)//kfz(111); krz[001]//kfz[11$\bar{2}$]) unter einachsiger Spannung, σ, senkrecht zur Grenzfläche wurde als Funktion der Atomplätze minimiert. Die Bindungsenergien wurden als Funktion des Keim-

radius', r, gefittet mit den Fitparametern der Grenzflächenenergie, γ, und Dehnungsenergie pro Raumeinheit, C.

Es ergab sich eine Abnahme der Grenzflächenenergie für zunehmenden einachsigen Zug. Die Ursache hierfür liegt in der Zunahme des Abstands zwischen Austenit- und Ferritatomen am Keimrande und in der daraus folgenden Abnahme der Abstoßung zwischen diesen Atomen. Für zunehmende einachsige Druckbelastung erreichte die Grenzflächenenergie ein Plateau, da in den Simulationsbedingungen ein Mindestabstand vorausgesetzt wurde. Die Grenzflächenenergie nahm zu mit zunehmender Keimdicke, da die relative Bedeutung der energetisch günstigen Wechselwirkungen zwischen Austenitatomen an der obersten Keimebene und energetisch günstigen Wechselwirkungen zwischen Ferritatomen an der untersten Keimebene abnahm.

Die Dehnungsenergie infolge der Volumensfehlpassung zwischen Ferrit und Austenit wurde mit Hilfe von Kontinuumsansätzen [3, 4] berechnet. Diese kontinuierlichen Methoden versagten jedoch bei der Vorhersage der Dehnungsenergie pro Volumeneinheit (cf. Fig. 5.3b). Dies ist eine Folge der Anwesenheit von freien Volumen an der Keimaußenkante, welche aufgrund des hohen Flächen / Volumenverhältnis solcher kleiner Partikel nicht vernachlässigt werden kann. Mit der aus der Simulation bestimmten Grenzflächenenergie und Dehnungsenergie ist es möglich, den kritischen Keimradius, r_c , und die damit verbundenen Keimbildungsenergie, ΔG^*, zu berechnen.

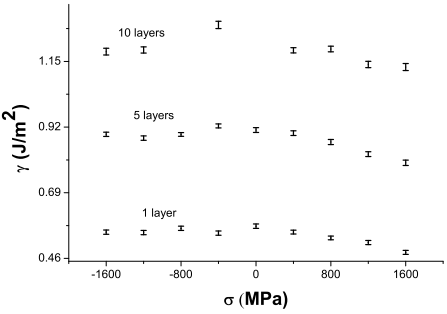

(a) γ

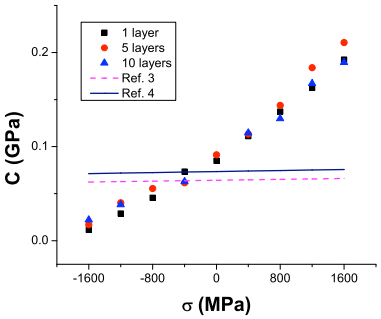

(b) C

Figure 5.3: die Grenzflächenenergie, γ (a), und die Dehnungsenergie, C (b), als Funktion der angelegten Spannung, σ. Die Fehlerbalken zeigen die Standardfehler für die Fits. Die Geraden in (b) zeigen die Vorhersage bon kontinuierlichen Methoden[3, 4].

5.4 Massive Austenit-Ferrit-Umwandlung unter Spannung

Grenzflächenkontrolliertes Ferritwachstum auf atomaren Zeit- und Längenskalen wurde mittels der multi-lattice kMC simuliert. Die untersuchten Systeme waren Bikristalle mit einem zweidimensionalen Keim an der Ferrit/Austenit-Grenzfläche. Es wurden Simulationen mit verschiedenen kristallografischen Orientierungsbeziehungen zwischen Ferrit und Austenit, unterschiedlichen Spannungszuständen, Dichten von Random Sites und Leerstelledichten ausgeführt. Mit den hierdurch bestimmten Umwandlungsraten wurde die Aktivierungsenergie für die Grenzflächenmobilität, ΔG^a, unter den verschiedenen Bedingungen berechnet.

Zumnächst wurde der Fall einachsige Spannung für zwei unterschiedliche Orientierungen untersucht. Im Fall von $\gamma(11\bar{2})//\alpha(111)$ wurde eher isotropisches Wachstum beobachtet, wohingegen im Fall von $\gamma(111)//\alpha(110)$ ein laterales Wachstum (senkrecht zur Belastungsrichtung) gefunden wurde. Die Umwandlungsrate der massiven Austenit-Ferrit-Umwandlung wurde durch Abfolgen von energetisch ungünstigen Sprüngen bestimmt, welche den benötigten Raum schaffen, um eine vorher durch Austenitatome blockierte leere Ferritstelle zugänglich zu machen. In Abwesenheit von Leerstellen hatte die angelegte einachsige Spannung keinen bedeutenden Einfluß auf die Aktivierungsenergie. Leerstellen vereinfachen die Umwandlung, wenn das mit Leerstellen assoziierte freie Volumen verfügbar ist. Andererseits blockieren Leerstellen die fortschreitende Grenzfläche, wenn Relaxation der Umgebung einer Leerstelle auftritt und mehr energetisch ungünstigen Sprungen benötigt sind um eine

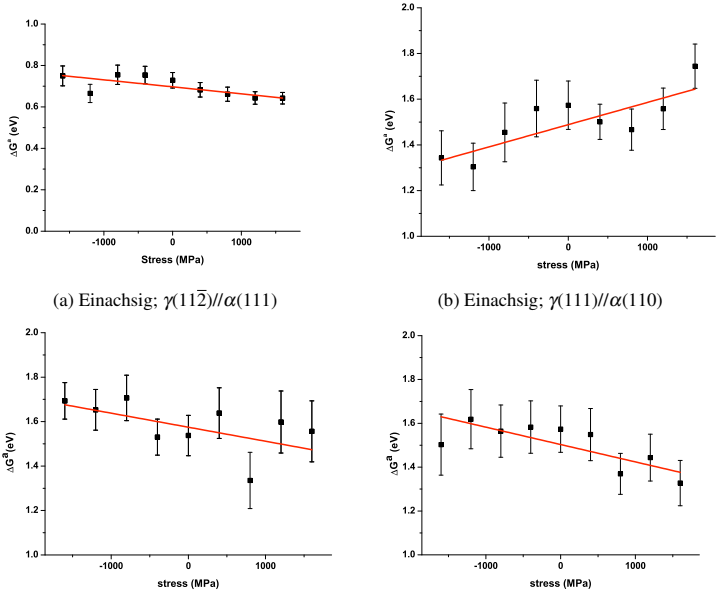

(a) Einachsig; $\gamma(11\bar{2})//\alpha(111)$

(b) Einachsig; $\gamma(111)//\alpha(110)$

(c) Zwei-achsig; $\gamma(111)//\alpha(110)$

(d) Hydrostatisch; $\gamma(111)//\alpha(110)$

Figure 5.4: Die Aktivierungsenergie für die Grenzflächenmobilität, ΔG^a, als Funktion der angelegten Spannung. Die Ergebnissen in (b), (c) und (d) basieren auf Simulationen für das System $\gamma(111)//\alpha(110)$ und 11 Leerstellen an der Grenzfläche. Die Ergebnissen in (a) basieren auf Simulationen für das System $\gamma(11\bar{2})//\alpha(111)$ und 5 Leerstellen an der Grenzfläche. Die Datenpunkte und die Fehlerbalken sind Ergebnisse und Standardfehler von nicht-linearem Fitting der Umwandlungsraten als Funktion der Temperatur. Die gerade Linien sind lineare Fits der Datenpunkte.

Leerstelle an der Grenzfläche zu verschieben. Der jeweils dominierende Effekt wird von der Leerstellenmobilität bestimmt. Bei anisotropem Wachstum fördert einachsiger Druck die Umwandlung wegen zunehmender Leerstellenmobilität in der Wachstumsebenen. Bei mehr isotropem Wachstum fordert einachsiger Zug die Umwandlung auf Grund des zunehmenden freien Volumens.

Für die $\gamma(111)//\alpha(110)$-Grenzfläche wurde die Umwandlung auch unter zweiachsiger (in der Wachstumsebene angelegt) und hydrostatischer Spannung simuliert. Bei Abwesenheit von Leerstellen hatte zweiachsige Spannung, wie bei einachsiger Spannung, keinen bedeutenden Einfluß auf ΔG^a. Bei hydrostatischem Druck hingegen nahm ΔG^a bedeutend zu, wohingegen bei hydrostatischem Zug ΔG^a bedeutend abnahm. Diese Zunahme ist Folge der gleichzeitig schrumpfenden Ebenenabstände der grenzflächenparallelen Ebenen und der zunehmenden Ebenendichte, welche beide die Umwandlung hemmen. Bei ein- und zweiachsiger Spannung wirken diese Effekten gegeneinander.

Bei Anwesenheit von Leerstellen an der Grenzfläche wurde die Umwandlung, wie auch im Fall von einachsiger Spannung, behindert, wenn die Ebenendichte in den Wachstumsebene infolge der angelegten Spannung zunahm, also bei einachsigem Zug und hydrostatischem und planarem Druck. Dies ist wiederum Folge der eingeschränkten Mobilität auf Grund von Relaxation der Umgebung einer Leerstelle an der Austenit-Ferrit-Grenzfläche.

REFERENCES

[1] H. I. Aaronson, C. Laird, and K. R. Kinsman, *Scr. Metall.*, 2(5):259 – 264, 1968.

[2] H. I. Aaronson, *Metall. Mater. Trans. A*, 33(8):2285–2297, 2002.

[3] F. R. N. Nabarro, *Proc. Phys. Soc.*, 52(1):90, 1940.

[4] E. Kröner, *Acta Metall.*, 2(2):302 – 309, 1954.

[5] C. Bos, F. Sommer, and E. J. Mittemeijer, *Acta Mater.*, 52(12):3545 – 3554, 2004.

[6] C. Bos, F. Sommer, and E. J. Mittemeijer, *Acta Mater.*, 53(20):5333 – 5341, 2005.

List of Publications

1. M. Biglari Jr. and E.J. Mittemeijer: Energetics of nucleation at the austenite-ferrite interface; the effect of applied stress. *Modelling and Simulation in Materials Science and Engineering*, **20**(7):075010, 2012. (Chapter 2 of this thesis)

2. M. Biglari Jr. and E.J. Mittemeijer: Simulation of the massive austenite-ferrite transformation under uniaxial loading. *Submitted for Publication*. (Chapter 3 of this thesis)

3. M. Biglari Jr. and E.J. Mittemeijer: Mobility of the austenite-ferrite interface under various states of loading. *Submitted for Publication*. (Chapter 4 of this thesis)

Curriculum Vitae

Personal Data

Name:	Mostafa Biglari
Date of Birth:	15th of December 1983
Place of Birth:	Teheran
Nationality:	Dutch, Iranian

Schooling

1987-1995	Primary school, A.M. de Jongschool, Delft, The Netherlands
1995-2001	High school, St. Stanislascollege (VWO), Delft, The Netherlands

Academic Education

2001-2008	Drs. Chemistry. University of Leiden, The Netherlands. Thesis: Simulation of Ca-treatment of Al-killed.
2005-2008	B.A. Philosophy of a scientific discipline. University of Leiden, The Netherlands. Thesis: Reflexive Predictions in Science.

Dissertation

2008-2012	Ph.D. at the Max Planck Insitute for Intelligent Systems (formerly Max Planck Insitute for Metals Research), Institute for Materials Science, University of Stuttgart and SimTech Cluster of Excellence, University of Stuttgart. Thesis: Simulation of the austenite-ferrite transformation; effect of stress.

Danksagung

Diese Doktorarbeit wurde am Max-Planck-Institut für Intelligente Systeme und am Institut für Materialwissenschaft, Universität Stuttgart, als Teil des Exzellenzclusters “SimTech” angefertigt. An dieser Stelle möchte ich allen danken, die zum Gelingen dieser Arbeit beigetragen haben.

Als erstes möchte ich Herrn Prof. Dr. Ir. Mittemeijer, meinem Doktorvater, danken für die Aufnahme in seine Abteilung und das Bereitstellen des Themas. Die vielen Diskussionen und die intensive Zusammenarbeit habe ich immer als sehr inspirierend, lehrreich und besonders angenehm erfahren. Ich bin dankbar für die Freiheit und die Möglichkeiten, die er mir geboten hat, um diese Arbeit auf meine Weise zu verwirklichen.

Der deutschen Forschungsgemeinschaft möchte ich herzlich danken für die finanzielle Unterstützung meiner Doktorarbeit im Rahmen des Exzellenzclusters “SimTech”.

Herrn. Prof. Dr. Schleid möchte ich für die Übernahme der Aufgabe als Prüfungsvorsitzender danken.

Herrn Prof. Dr. Schmauder möchte ich für die Mitbetreunung und die Übernahme des Mitberichts dieser Arbeit danken. Die tiefen Diskussionen mit ihm und seinen Mitarbeitern waren wichtig für das Erweitern meines Verständnisses

bezüglich Simulationstechniken.

Natürlich war die Durchführung der Arbeit nicht möglich ohne meine Arbeitskollegen beim Max-Planck-Institut als auch bei SimTech, die mich täglich unterstützt haben und für eine angenehme Arbeitsatmosphäre sorgten. Besonders dankbar bin ich Markus, Wolfgang, Rico und Matthias die während meines Beinbruchs durch ihre Hilfsbereitschaft das Weiterarbeiten ermöglicht hatten.

برای کمک فراوان از خانواده بیگلری، فخیم طالبیان، اردبیلی اصل و حاج حیدری خیلی ممنونم.

Graag wilde ik op deze plaats mijn ouders en mijn zus danken voor de ondersteuning die zij op elk vlak hebben geboden.

Elnaz, dich während meiner Zeit in Stuttgart zu finden, war das Beste was mir je passieren konnte. Ich bin dir dankbar für deine Liebe und deinen Rückhalt.